Summer 2014

Heterogeneous reaction and kinetics of acetic acid on components of mineral dust aerosol

Whitney Anne Larish
University of Iowa

HETEROGENEOUS REACTION AND KINETICS OF ACETIC ACID ON COMPONENTS OF MINERAL DUST AEROSOL

by

Whitney Anne Larish

A thesis submitted in partial fulfillment
of the requirements for the
Master of Science degree in Chemistry
in the Graduate College of The University of Iowa

August 2014

Thesis Supervisor: Professor Vicki H. Grassian

Graduate College
The University of Iowa
Iowa City, Iowa

CERTIFICATE OF APPROVAL

MASTER'S THESIS

This is to certify that that Master's thesis of

Whitney Anne Larish

has been approved by the Examining Committee for the thesis requirement for the Master of Science degree in Chemistry at the August 2014 graduation.

Thesis Committee: _____
Vicki H. Grassian, Thesis Supervisor

_____
Sarah C. Larsen

_____
Tori M. Forbes

ACKNOWLEDGEMENTS

First, I would like to thank Professor Vicki H. Grassian for all of her support and guidance in making my research a success. I would also like to thank Professor Sarah Larsen and Professor Tori Forbes for their support and the National Science Foundation for funding my research.

I would like to thank former and current Grassian group members for the support I have received throughout my time here, with special thanks going to Dr. Gayan Rubasinghege for being a great mentor, and Aruni Gankanda and Dr. Charith Nanayakkara for their help and support.

I am grateful for the unconditional support I received from all of my friends, with special thanks to Ariel Bohman, Hannah Rosenthal, and Nick Janiczek for helping me achieve my goals. The emotional support I received from my family has been imperative to my success and for that I must give them the biggest thanks.

TABLE OF CONTENTS

LIST OF TABLES v

LIST OF FIGURES vi

CHAPTER

1. INTRODUCTION 1

2. EXPERIMENTAL MATERIALS AND METHODS 6

   2.1 Materials 6
   2.2 Sample Preparation 7
   2.3 Transmission Fourier Transform Infrared (FT-IR) Spectroscopy 10

3. HETEROGENEOUS REACTION AND SATURATION COVERAGE OF ACETIC ACID ON γ-Al_2O_3, SiO_2 AND CaO SURFACES 12

   3.1 Introduction 12
   3.2 Experimental Procedure 12
   3.3 Results and Discussion 14
      3.3.1 Surface Adsorption Modes of Acetic Acid on Oxide Surfaces 18
      3.3.2 Determination of Saturation Coverage 26
   3.4 Conclusions 29

4. REACTION KINETICS OF ACETIC ACID ON γ-Al_2O_3 UNDER DRY CONDITIONS AND EFFECT OF RELATIVE HUMIDITY ON UPTAKE 34

   4.1 Introduction 34
   4.2 Experimental Procedure 34
      4.2.1 Kinetics Experiments under Dry Conditions 34
      4.2.2 Kinetics Experiments in the Presence of Water 35
   4.3 Results and Discussion 36
   4.4 Conclusions 43

5. CONCLUSION 44

APPENDIX..46

REFERENCES...50

LIST OF TABLES

Table 2.1. Characterization of laboratory proxies of mineral dust components. 6

Table 3.1. Vibrational mode assignments of gas phase acetic acid. 16

Table 3.2. Vibrational mode assignments for weakly adsorbed acetic acid on γ-Al_2O_3, SiO_2 and CaO... 23

Table 3.3. Vibrational mode assignments for strongly adsorbed acetic acid on γ-Al_2O_3, SiO_2 and CaO.. 24

Table 3.4. Saturation coverage of acetic acid on γ-Al_2O_3, SiO_2 and CaO. 33

Table 4.1. Kinetics analysis of acetic acid uptake averages on γ-Al_2O_3 under dry conditions and in the presence of water vapor 41

Table A.1. Kinetics analysis of acetic acid uptake on γ-Al_2O_3 under dry conditions and in the presence of water vapor 46

LIST OF FIGURES

Figure 2.1. Sample chamber apparatus. (a) Schematic of sample holder with tungsten mesh grid and example of sample application and (b) sample chamber. 8

Figure 2.2. Schematic of FT-IR system equipped with turbo/mechanical pump system and water and acetic acid bulbs. 9

Figure 3.1. FT-IR absorbance spectrum of gas phase acetic acid at 1500 mTorr. 15

Figure 3.2. Structures of acetic acid in the gas phase. (a) Acetic acid monomer and (b) acetic acid dimer. 16

Figure 3.3. FT-IR spectra of (C=O) for the acetic acid monomer and dimer with increasing gas-phase acetic acid pressures. Pressures displayed in (a) are 60, 70, 80, 90, 100, 150, 200, 300, 500, 800 and 1500 mTorr, while (b) shows 60, 70, 80, 90, 100, 150, 200 mTorr. 17

Figure 3.4. FT-IR absorbance spectra of γ-Al_2O_3 with gas phase subtracted. (a) Full spectral range (800-4000 cm^{-1}) (b) 800-1900 cm^{-1}, with the top spectrum of each displaying the surface spectrum with the gas phase evacuated. 20

Figure 3.5. FT-IR spectra of SiO_2 with gas phase subtracted. (a) Full spectral range (1275-4000 cm^{-1}) (b) 1275-1900 cm^{-1}, with the top spectrum of each displaying the surface spectrum with the gas phase evacuated. 21

Figure 3.6. FT-IR spectra of CaO with gas phase subtracted. (a) Full spectral range (800-4000 cm^{-1}) (b) 800-1900 cm^{-1}, with the top spectrum of each displaying the surface spectrum with the gas phase evacuated. 22

Figure 3.7. Visual depiction of acetic acid coordination on oxide surfaces. (a) Bidentate coordination and (b) monodentate coordination. 25

Figure 3.8. Plots used to calculate saturation coverage. (a) Calculated surface coverage versus pressure and (b) [P/N] versus pressure for γ-Al_2O_3 using peak height of band at 1586 cm^{-1}. 30

Figure 3.9. Plots used to calculate saturation coverage. (a) Calculated surface coverage versus pressure and (b) [P/N] versus pressure for SiO_2 using the integrated area of the C=O stretching modes. 31

Figure 3.10. Plots used to calculate saturation coverage. (a) Calculated surface coverage versus pressure and (b) [P/N] versus pressure for CaO using the integrated area of peaks at 1613 and 1711 cm^{-1}. 32

Figure 4.1. Absorbance FT-IR spectra of acetic acid adsorption, 70 mTorr, on γ-Al_2O_3 with increasing time. 38

Figure 4.2. Absorbance FT-IR spectra of acetic acid adsorption, 150 mTorr, on γ-Al_2O_3 with increasing time. 39

Figure 4.3. Absorbance FT-IR spectra of acetic acid adsorption, 300 mTorr, on γ-Al_2O_3 with increasing time. 40

Figure A.1. FT-IR spectra of γ-Al_2O_3 in presence of 70 mTorr acetic acid and 5% relative humidity. (a) Full spectral range (800-4000 cm^{-1}) and (b) 800-1900 cm^{-1}. 47

Figure A.2. FT-IR spectra of γ-Al_2O_3 in presence of 150 mTorr acetic acid and 5% relative humidity. (a) Full spectral range (800-4000 cm^{-1}) and (b) 800-1900 cm^{-1}. 48

Figure A.3. FT-IR spectra of γ-Al_2O_3 in presence of 300 mTorr acetic acid and 5% relative humidity. (a) Full spectral range (800-4000 cm^{-1}) and (b) 800-1900 cm^{-1}. 49

CHAPTER 1

INTRODUCTION

Over time the atmosphere that surrounds us and its components have changed. As humans have traversed new land and made new industrial discoveries, the atmosphere has become a complex mixture containing a wide variety of particles and gases. Additionally, constituents have a significant effect on processes and reactions that occur within the atmosphere. It is important to understand these processes and reactions in order to properly assess and understand the Earth's atmosphere in terms of atmospheric chemistry and climate. Among the particles found in the atmosphere, mineral dust aerosol is ubiquitous. When considering atmospheric gases, there is a wide range of gases including O_2, N_2, H_2O, CO_2, SO_2, O_3 and NO_x, as well as both inorganic and organic acids such as nitric acid (HNO_3), formic acid (HCOOH) and acetic acid (CH_3COOH). Each of these acidic gases is found in trace amounts compared to the gases that comprise the majority of the atmosphere, such as O_2 and N_2. These trace gases tend to be very reactive, therefore, studies that address their reactivity in the atmosphere are imperative.

Due to the wide variety of chemical compositions that make up mineral dust aerosol, the term mineral aerosol is too vague and does not accurately describe the rich mineralogy and chemical composition. Tong et al. describes

mineral aerosol as fine particles originating from the earth's crust and generated by wind erosion.[1] The regions where mineral aerosol generate from tend to be mostly arid regions, where coverage of the land by vegetation is sparse, which make up one third of the earth's land surface.[2,3] The amount of mineral aerosol emitted into the atmosphere annually has been found to range from 1,000 – 3,000 Tg yr^{-1}.[3,4,5,6] However, the emission of mineral dust aerosol into the atmosphere at any one moment in time is dependent on a variety of factors including changes in land use due to mining/industrial activities, erosion, and overgrazing as well as shifting patterns in precipitation.[7]

The effects of mineral dust aerosol on the climate of the atmosphere are plentiful. Direct climate effects of mineral dust aerosol include its ability to absorb and scatter both solar and thermal radiation, having both warming and cooling effects, while it indirectly effects the climate by acting as cloud condensation nuclei (CCN).[1,4,8,9] Studies have also shown that they play an important role in atmospheric chemistry through the promotion of heterogeneous reactions.[4,10] By providing reaction sites and serving as carriers, mineral dust aerosol has the ability to control the concentration, lifetime, and physical and chemical behavior of a variety of biogeochemicals such as carbon, nitrogen and sulfur.[10] The particles' capacity to engage in such reactions is dependent on multiple factors. As to be expected from a natural material, not

every particle that mineral dust is composed of has the exact same size, physical properties, or chemical composition. Reactivity within the atmosphere depends greatly on the chemical composition of the particles as well as the size, which effects the length of time that the particle remains suspended in the atmosphere.[2] The smaller the particle, the more likely it is to have a longer lifetime in the atmosphere. Not only does this give the particle more time to react with atmospheric trace gases, but it also allows for the particle to potentially move farther away from the source region compared to its larger counterpart.

The reaction between acid vapor and mineral dust particles in the atmosphere is an important interaction to consider. Previous studies[11,12] have shown that acids have the ability to react with various components of mineral dust aerosol to varying extents. Organic acids in particular have become a focus in recent years due to their universal presence in the atmosphere, with emphasis on formic and acetic acid. Formic acid and acetic acid are the first and second most abundant organic acids in the atmosphere, respectively, and have been found in concentrations varying from 0.1 to 40 ppbv for formic acid and 0.5 to 16 ppbv for acetic acid.[13] Both acids have been found in all types of precipitation including fog, cloud, rain, snow and ice water, in addition to contributing 16 to 35% of the free acidity in precipitation in the United States.[13]

Carboxylic acids found in the atmosphere come from a wide range of sources including various anthropogenic and biogenic emissions.[13] Some examples of direct emission from anthropogenic sources include plastics combustion, chemical plant emission and refuse incineration factories, among others.[13] Biomass burning, through events such as wood burning stoves, forest fires and agricultural burnings, have also been shown to be a direct source of anthropogenic emission, with acetic acid emission being favored over formic acid emission at a ratio of two to ten.[14] Another important source of carboxylic acids in the atmosphere is motor exhaust emission. The distribution of acids in motor exhaust emission is similar to that found in air, however, it was determined that the concentration of acetic acid was nearly 17 times higher.[14] Biogenic emissions consist primarily of soil and vegetation emission and tend to favor the emission of acetic acid.[13] This type of emission is a more prevalent source in forested regions where vegetation is dense, with acids such as acetic, formic and pyruvic acids being emitted directly from the leaves of trees.[13]

The scope of the research presented here focuses specifically on the interaction between acetic acid and laboratory proxies representing three components of mineral dust aerosol, γ-Al_2O_3, SiO_2 and CaO. Transmission Fourier transform infrared (FT-IR) spectroscopy was used to investigate the surface adsorption modes and determine the saturation coverage of acetic acid

on each component under dry conditions. In addition, the initial uptake kinetics of acetic acid on γ-Al_2O_3 were studied under both dry and humid conditions in order to study the effect of water on initial acetic acid uptake.

CHAPTER 2

EXPERIMENTAL MATERIALS AND METHODS

2.1. Materials

The oxide particles used in this study are laboratory proxies for different components of mineral dust aerosol. Information regarding the chemical composition and source of these proxies as well as the BET (Brunauer-Emmett-Teller) surface area is provided in Table 2.1. The γ-Al_2O_3 and SiO_2 samples were purchased from Degussa Chemical and CaO sample was purchased from Alfa Aesar. Each sample was pressed onto one half of a tungsten grid for spectroscopic studies. Samples were then placed in the sample cell and the system was allowed to evacuate for six hours for kinetic studies and overnight for saturation studies as detailed in chapters 3 and 4.

Table 2.1. Characterization of laboratory proxies of mineral dust components.

Sample	Commercial Source	Surface Area (m^2/g)
γ-Al_2O_3	Degussa Chemical (Aluminum Oxide C)	101 (± 4)
SiO_2	Degussa Chemical (OX-50)	50 (± 6)
CaO	Alfa Aesar (Lot #10923)	3.9 (± 0.5)

Throughout this project, glacial acetic acid purchased from Alfa Aesar (Lot #F12N44) was used. For transmission FT-IR studies, acetic acid was placed in a long-neck glass bulb with outlet. The acid was degassed by a freeze-pump-

thaw process. First, the acid was frozen slowly using liquid nitrogen before attaching the bulb to the pump system to evacuate any water vapor that was produced as the acid thawed. Once the acid had thawed, the bulb was removed from the pump system. This freeze-pump-thaw process was performed a total of three times to ensure that all water vapor had been removed from the bulb.

For studies involving relative humidity, optima water was placed in a long-neck glass bulb with outlet and degassed by the same freeze-pump-thaw process described for the acetic acid. The procedure was repeated a total of five times to ensure all contaminants were removed.

2.2. Sample Preparation

Samples were prepared by pressing the oxide of interest to one half of a clean, dry tungsten grid as shown in Figure 2.1a. The grid was then secured in a set of nickel jaws attached to the lid of the sample cell. Once the sample was placed in the sample chamber and the lid was sealed, the entire system was allowed to evacuate under vacuum for a minimum of six hours prior to performing an experiment. Prior to experimentation, spectra were collected of both the sample and the tungsten grid while still under vacuum using the linear translator. These single beam spectra were then used as reference spectra to determine the surface spectra during and after experimentation. Taking the negative log of the ratio of the single beam spectrum of the sample and the single

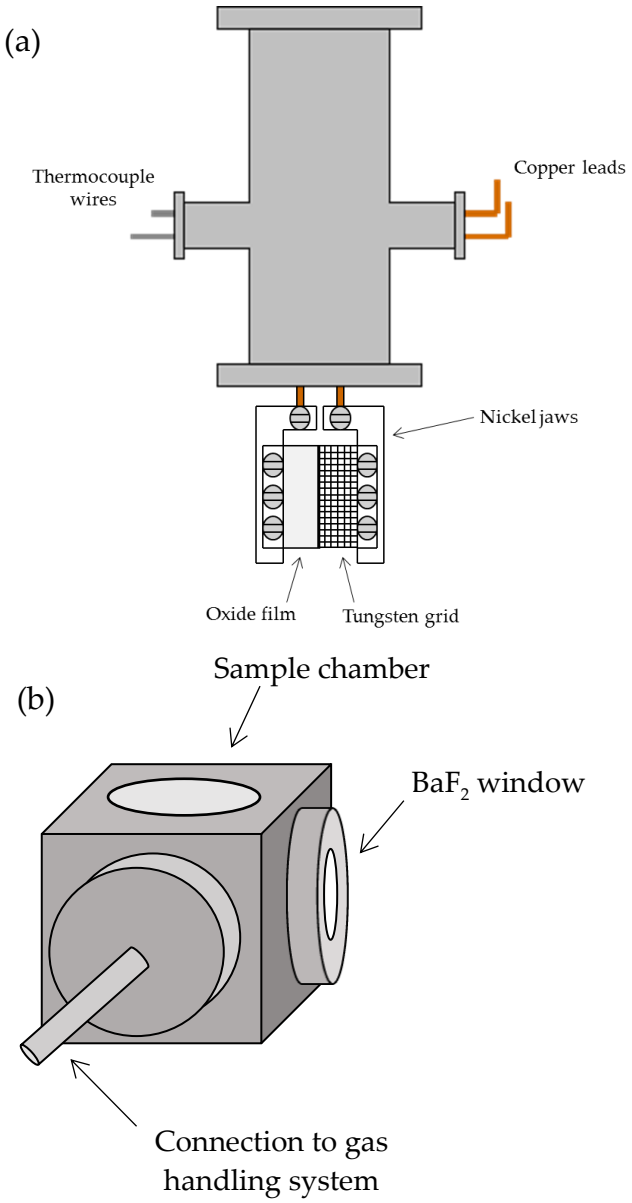

Figure 2.1. Sample chamber apparatus. (a) Schematic of sample holder with tungsten mesh grid and example of sample application and (b) sample chamber.[15]

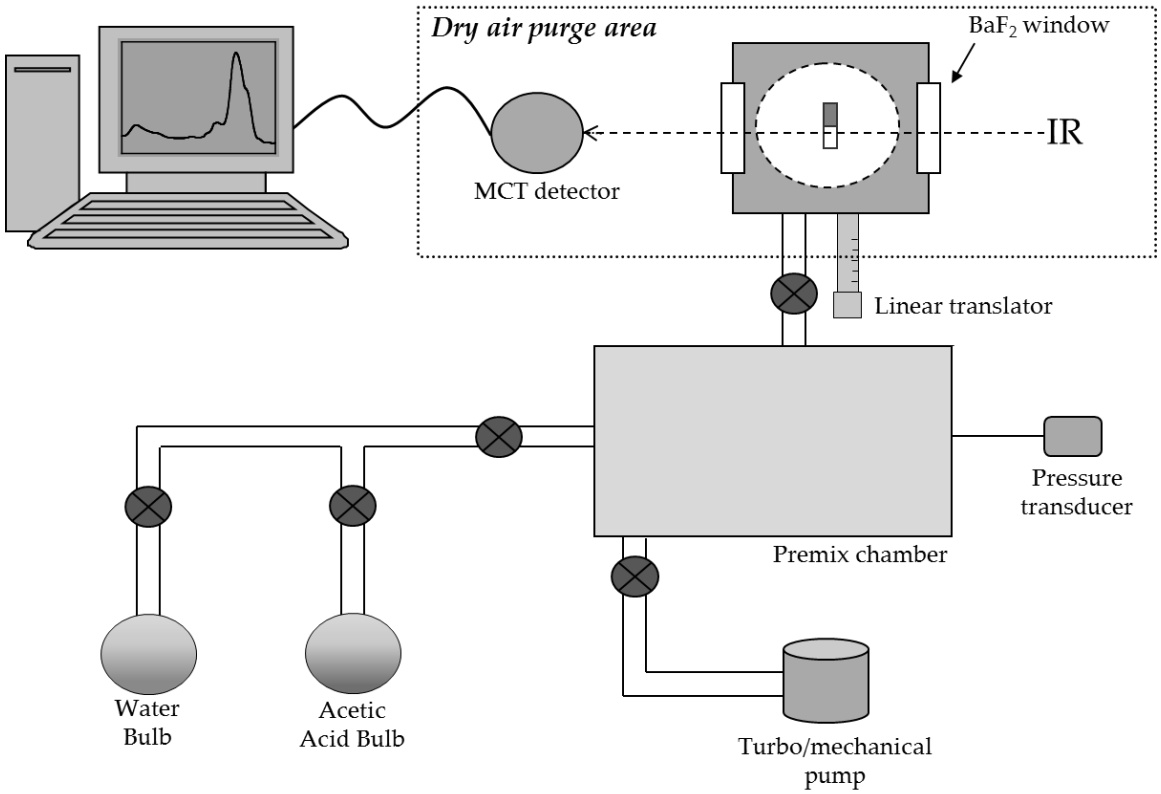

Figure 2.2. Schematic of FT-IR system equipped with turbo/mechanical pump system and water and acetic acid bulbs.[15]

beam spectrum of the tungsten grid provides an absorbance spectrum of the clean, dry sample.

2.3 Transmission Fourier Transform Infrared (FT-IR) Spectroscopy

A custom vacuum system connected to a Mattson GL-6021 FT-IR Spectrometer in conjunction with a mercury-cadmium-telluride (MCT) detector was used. The sample chamber shown in Figure 2.1b was equipped with two BaF_2 windows and stainless steel tubing leading to the gas handling system. The chamber was mounted on a linear translator to allow spectra to be collected for both the sample and the tungsten grid. A schematic of the entire system is shown in Figure 2.2.

Within the WinFirst software, absorbance spectra of both the sample and gas phase were collected. The single beam spectra of the clean sample and tungsten grid collected after evacuation of the system were used as background spectra. Transmittance spectra were calculated by taking the ratio of the experimental single beam spectrum and the respective background spectrum, sample or gas phase. Using the relation that $A = \log_{10}(100/\%T)$, where A is absorbance and %T is percent transmittance, absorbance spectra of the surface and gas phase were calculated. The absorbance spectrum of the gas phase was then subtracted from the absorbance spectrum of the sample to create an absorbance spectrum of the sample surface only. This subtraction of spectra was

performed for saturation studies to investigate the surface adsorption. For saturation studies, 250 scans were collected from 800 to 4000 cm^{-1} with a resolution of 4 cm^{-1}, while the kinetics studies required only four scans so that spectra could be collected at a faster rate. Relative humidity studies required spectra to be collected at an even faster rate than the kinetics studies, so only one scan was collected per spectrum with a resolution of 8 cm^{-1}. The FT-IR system where the sample cell was held was purged with dry air to eliminate carbon dioxide from the sample spectra.

CHAPTER 3

HETEROGENEOUS REACTION AND SATURATION COVERAGE OF ACETIC ACID ON γ-Al_2O_3, SiO_2 AND CaO SURFACES

3.1. Introduction

The first step in understanding the reactivity of acetic acid on the oxide surfaces is analyzing the FT-IR spectra to determine the nature of the species present. Previous studies of nitric acid adsorption on various components of mineral dust aerosol have shown irreversible absorption on both alumina and calcium oxide surfaces, in addition to reversible adsorption on the silica surface.[11] The coordination of the adsorbed species on the surface can also be determined through the analysis of the FT-IR spectra. Due to the complexity of acetic acid in the gas phase, comparison of the sample spectra to the spectrum of gas phase acetic acid provides information about whether the acetic acid monomer or dimer is adsorbed on the surface. Once these species are identified, the spectra can be used to determine the coverage of acetic acid on the surface. By plotting surface coverage at various acetic acid pressures versus pressure, the saturation coverage of acetic acid on each component can be determined.

3.2. Experimental Procedure

For studies to determine the saturation coverage of acetic acid on each oxide in question, the following procedure was followed. First, the premix

chamber (as defined in Figure 2.2) was isolated from both the pumping system and the sample chamber. Acetic acid was then introduced into the premix chamber where a pressure transducer was used to monitor the pressure within the chamber until the desired pressure was reached. After allowing the pressure to stabilize, the valve separating the sample chamber and premix chamber was opened, exposing the sample to the acetic acid. Upon introduction of acetic acid to the sample chamber the pressure would decrease. After 20 minutes this equilibrium pressure was recorded and spectra were collected of both the sample and tungsten grid with the gas phase still present. The system was then evacuated under vacuum for 20 minutes before collecting subsequent spectra of the sample and tungsten grid. This procedure was then repeated for each desired pressure. The initial pressures γ-Al_2O_3 and CaO were exposed to included 0.070, 0.080, 0.090, 0.100, 0.150, 0.200, 0.300, 0.500, 0.800, and 1.500 Torr. For SiO_2, the initial exposure pressures were 0.060, 0.070, 0.080, 0.090, 0.100, 0.200, 0.300, 0.500, 0.800, and 1.500 Torr. After exposure to the final pressure, the system was allowed to evacuate under vacuum overnight. After this final evacuation, but before removing the sample, spectra of the sample and tungsten grid were collected one last time to provide information about which species strongly adsorb on the various oxide surfaces.

3.3. Results and Discussion

Before identifying the surface adsorption modes of acetic acid on the three different oxide surfaces it is important to consider the vibrational modes of acetic acid. The FT-IR spectrum of gas phase acetic acid at the highest pressure studied, 1500 mTorr, is shown in Figure 3.1 along with vibrational mode assignments in Table 3.1. The hydroxyl stretching and bending modes can be clearly identified at 3580 and 1295 cm^{-1} respectively. There are distinct bands in the C-H stretching region as well as distinct peaks at 1426 and 1176 cm^{-1} representing the CH_3 bending and C-O stretching modes. Acetic acid in the gas phase is known to exist as both a monomer and dimer, the structures of which are shown in Figure 3.2. These two structures result in two carbonyl stretching modes at 1790 cm^{-1} and 1733 cm^{-1}, representing the monomer and dimer respectively. At higher pressures (>500 mTorr), as shown by Figure 3.3a, the dimer appears to be more abundant than the monomer based on peak height of these two bands.

Comparing these two peaks at lower pressures (≤300 mTorr), the monomer is present as the more abundant species as seen in Figure 3.3b. Calculation of the relative abundance of each species at the three pressures used during the kinetics studies reveal that approximately 75-90% of acetic acid at each pressure remained in the monomeric form. Therefore, it is appropriate to

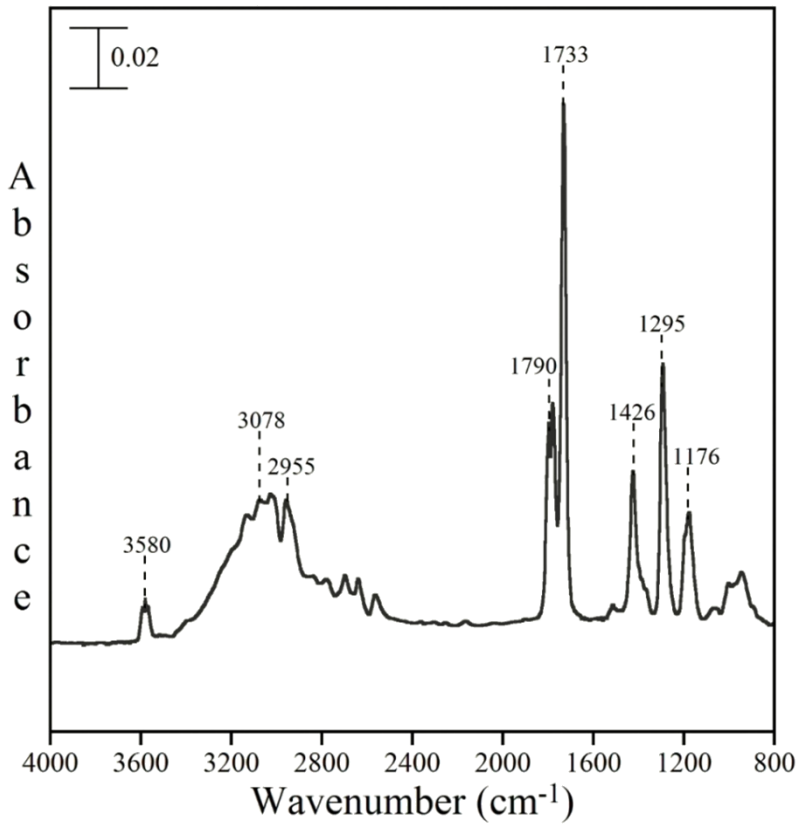

Figure 3.1. FT-IR absorbance spectrum of gas phase acetic acid at 1500 mTorr.

Table 3.1. Vibrational mode assignments of gas phase acetic acid.

Mode Assignment	This work	Literature
ν (OH)	3580	3583[17]
ν (CH)	3078, 2955	2996[17], 2944[17]
ν $(C=O)_{monomer}$	1790	1788[17], 1776[18]
ν $(C=O)_{dimer}$	1733	1733[19], 1729[18]
δ (CH_3)	1426	1424[18]
δ (OH)	1295	1292[18]
ν (C-O)	1176	1180[17]

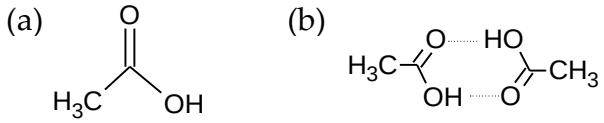

Figure 3.2. Structures of acetic acid in the gas phase. (a) Acetic acid monomer and (b) acetic acid dimer.

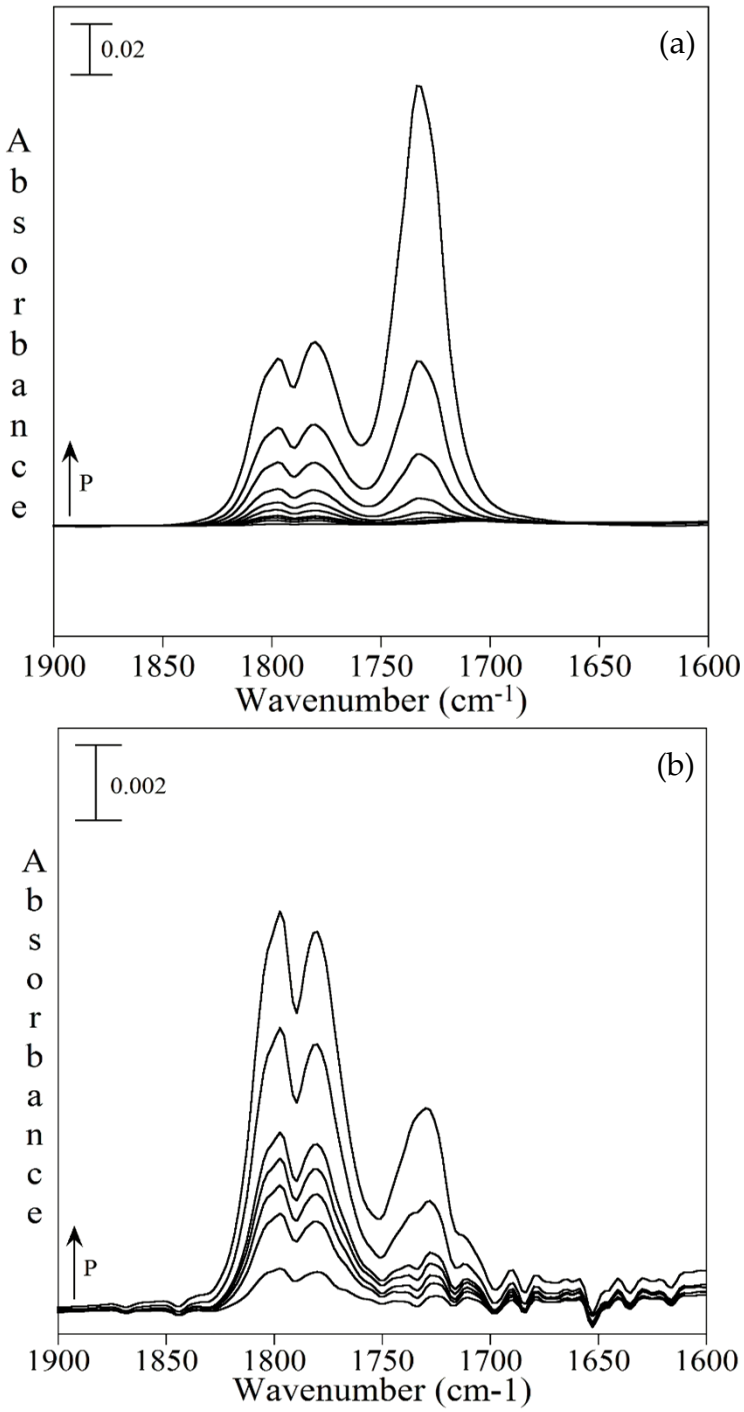

Figure 3.3. FT-IR spectra of (C=O) for the acetic acid monomer and dimer with increasing gas-phase acetic acid pressures. Pressures displayed in (a) are 60, 70, 80, 90, 100, 150, 200, 300, 500, 800, and 1500 mTorr, while (b) shows 60, 70, 80, 90, 100, 150, and 200 mTorr.

assume that only the monomer is present when calculating flux. However, it is important to acknowledge there is error in this value due to the presence of dimer that is not accounted for.

3.3.1. Surface Adsorption Modes of Acetic Acid on Oxide Surfaces

Figures 3.4, 3.5, and 3.6 show the infrared spectra of the γ-Al_2O_3, SiO_2, and CaO surfaces after exposure to ten different pressures of acetic acid as well as after evacuation of acetic acid from the system. These surface spectra were created by subtracting the gas phase spectrum from the spectrum collected of the surface when the gas phase was present. By doing so, the bands remaining in the figures represent only adsorbed surface species. The spectra labeled "gas phase evacuated" were created using the spectra of the surface collected after the final pressure was introduced and the system was evacuated. The pressures at which each spectrum was collected for γ-Al_2O_3 were 0.002, 0.013, 0.020, 0.026, 0.047, 0.070, 0.122, 0.230, 0.397, and 0.801 Torr, while for CaO, the pressures at which each spectrum was collected were 0.003, 0.012, 0.019, 0.025, 0.045, 0.070, 0.122, 0.228, 0.395, and 0.790 Torr. For SiO_2, the pressures at which each spectrum was collected were 0.002, 0.013, 0.018, 0.023, 0.027, 0.072, 0.123, 0.233, 0.403, and 0.802 Torr.

Considering γ-Al_2O_3, it is seen that the reaction of acetic acid on the surface is largely irreversible, as indicated by the presence of peaks remaining in

the spectrum after evacuation of the gas phase. However, there are some adsorption bands that disappear following gas phase evacuation. This suggests that acetic acid is both strongly and weakly adsorbed on the surface. This pattern is also seen for adsorption on SiO_2 and CaO in figures 3.5 and 3.6, but with varying amounts of reversible and irreversible surface adsorption. Vibrational mode assignments for both weakly and strongly adsorbed acetic acid on the surface are listed in Tables 3.2 and 3.3.

The negative bands at 3698 and 3742 cm^{-1} in the γ-Al_2O_3 and SiO_2 spectra respectively have been shown to be indicative of the interaction with or loss of surface hydroxyl groups which can be described by the reaction shown by equation 3.1.[12] The multi-peak above 2500 cm^{-1} in the spectra with the gas phase present are also indicative of hydrogen bonding of acetic acid to the surface.[16]

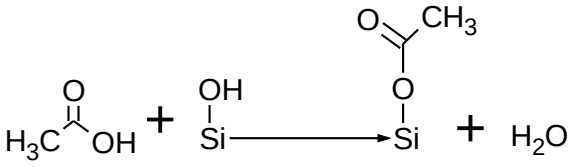

(3.1)

The γ-Al_2O_3 and SiO_2 spectra also clearly show that both the monomer and dimer phases of acetic acid are present as evidenced by the ν(C=O) modes at 1758 and 1716 cm^{-1} for the monomer and dimer respectively.[16] The vibrational mode at 1711 cm^{-1} in the CaO spectra also represents the acetic acid monomer. Upon evacuation, these peaks disappear, indicating physisorption of acetic acid

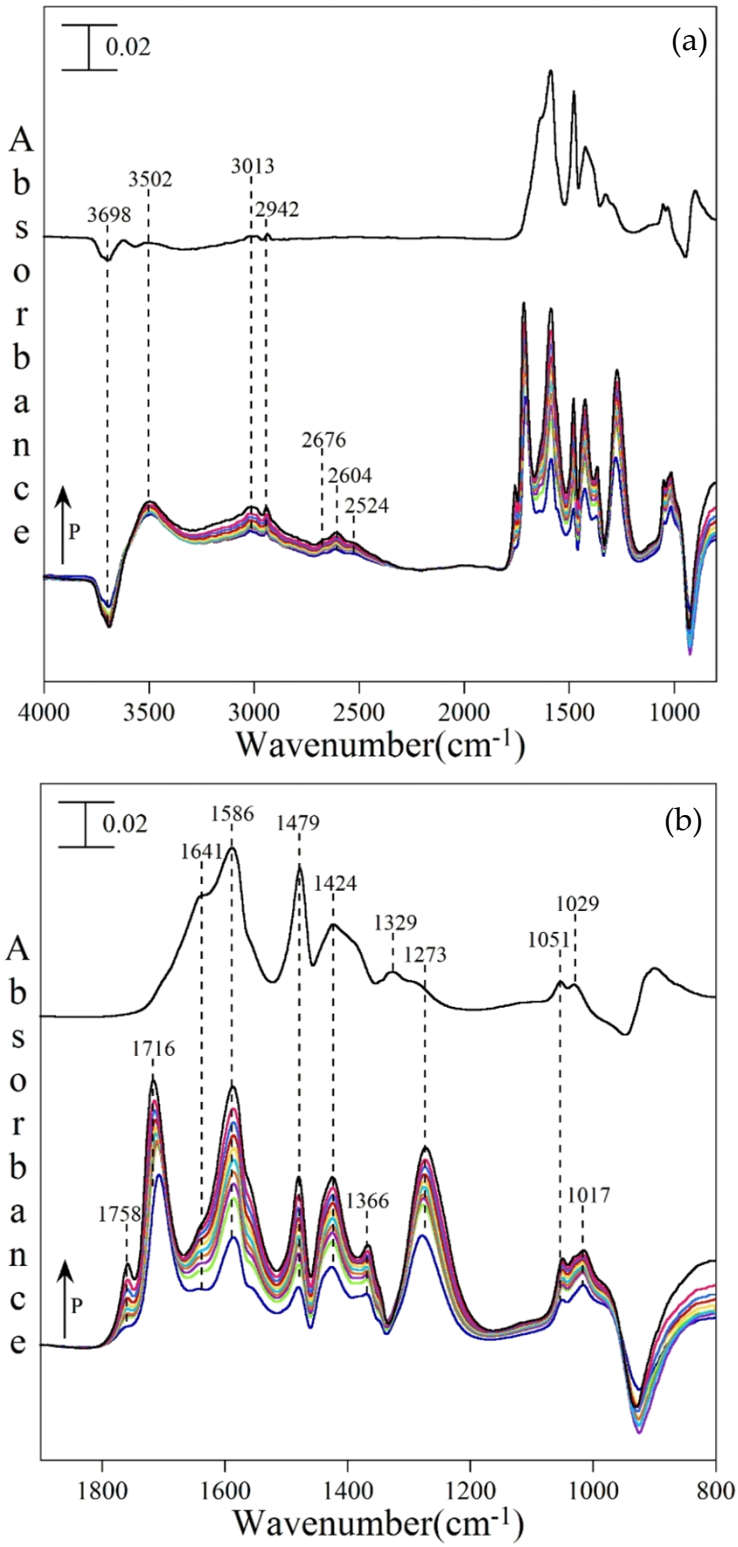

Figure 3.4. FT-IR absorbance spectra of γ-Al_2O_3 with gas phase subtracted. (a) Full spectral range (800-4000 cm^{-1}) (b) 800-1900 cm^{-1}, with the top spectrum of each displaying the surface spectrum with the gas phase evacuated.

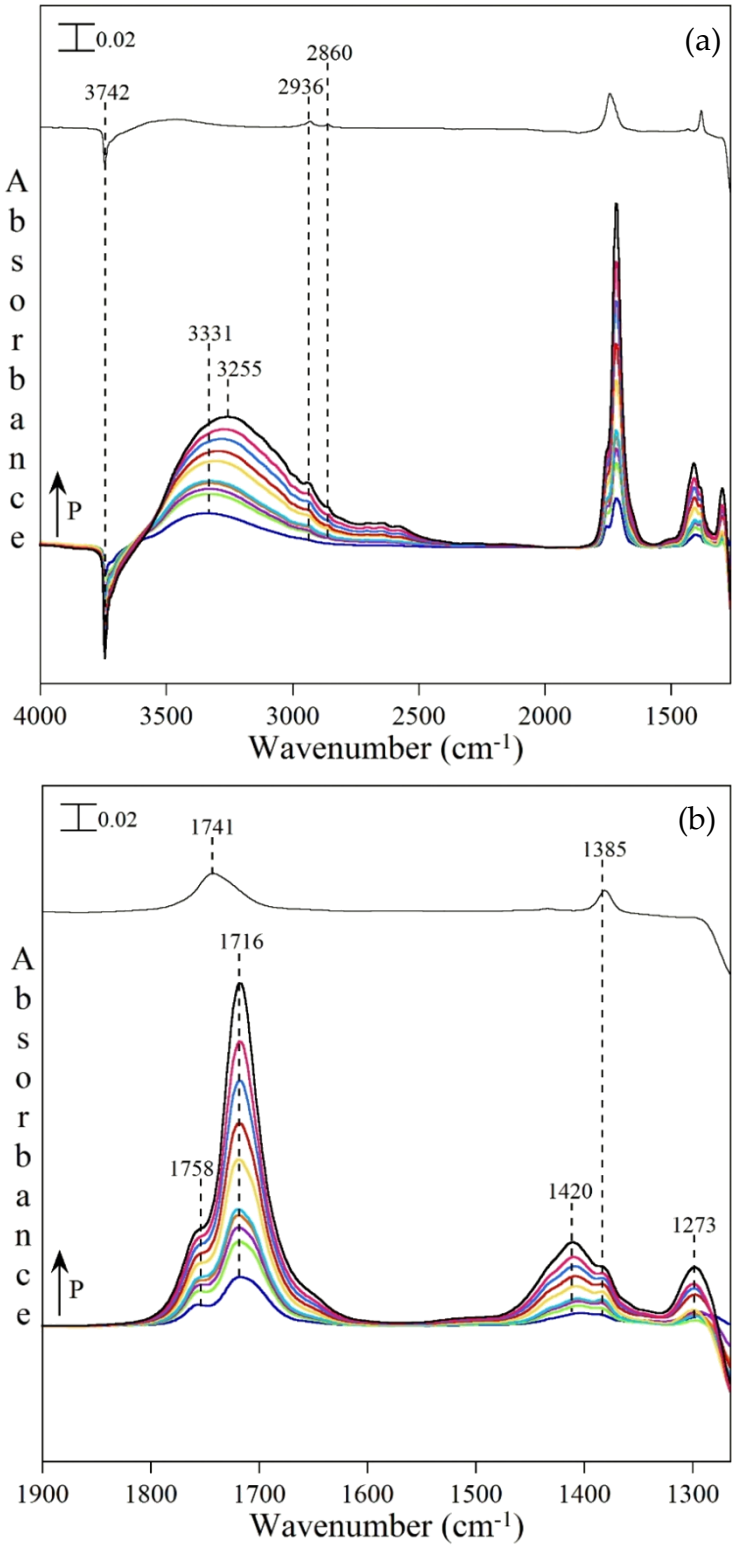

Figure 3.5. FT-IR spectra of SiO_2 with gas phase subtracted. (a) Full spectral range (1275-4000 cm^{-1}) (b) 1275-1900 cm^{-1}, with the top spectrum of each displaying the surface spectrum with the gas phase evacuated.

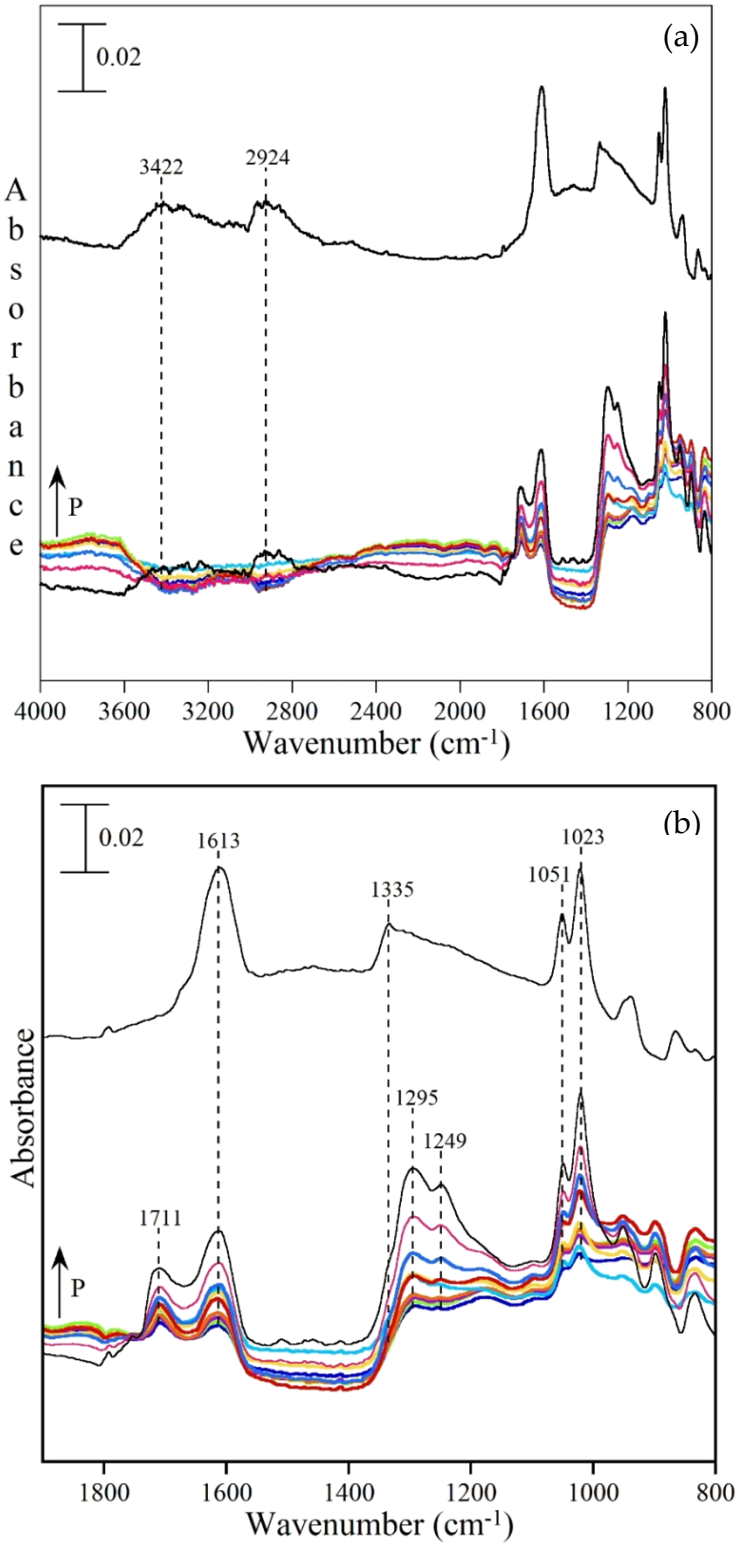

Figure 3.6. FT-IR spectra of CaO with gas phase subtracted. (a) Full spectral range (800-4000 cm^{-1}) (b) 800-1900 cm^{-1}, with the top spectrum of each displaying the surface spectrum with the gas phase evacuated.

Table 3.2. Vibrational mode assignments for weakly adsorbed acetic acid on γ–Al_2O_3, SiO_2 and CaO.

	Mode Assignment	**γ-Al_2O_3**	**SiO_2**	**CaO**	**Acetic Acid (gas phase)**
Weakly Bound CH_3COOH	ν_s (OH)	3502	3331	3422	3583[17]
	$\nu_{as/s}$ (CH_3)	2942	2936	2924	2944[17], 2996[17]
	ν $(C=O)_{monomer}$	1758	1758		1788[17], 1776[18]
	ν $(C=O)_{dimer}$	1716	1716	1711	1733[19], 1729[18]
	δ (CH_3)	1366, 1424	1385, 1420		1382[17], 1424[18]
	δ (OH) & ν (C-O)	1273	1273	1249, 1295	1264[17], 1292[18]

Table 3.3. Vibrational mode assignments for strongly adsorbed acetic acid on γ–Al_2O_3, SiO_2 and CaO.

	Mode Assignment	**γ-Al_2O_3**	**SiO_2**	**CaO**	**Literature Values**
Hydroxyl groups and acetate	ν(OH)	-3698[a]	-3742[a], 3255		-3744[a,11], 3251[11]
	δ(OH)				1279[16], 1302[16]
Strongly Bound Acetate Species	$\nu_{as/s}(CH_3)$	2942			2935[20]
	$\nu(C=O)_{monomer}$		1741		1746[16]
	$\nu(C=O)_{dimer}$				1701[16]
	$\nu_{as}(COO)$	1586, 1641		1613	1590[18], 1630[19]
	$\nu_{s}(COO)$	1479, 1329		1335	1470[18], 1323[19]
	$\delta(CH_3)$	1424			1432[16], 1340[20], 1420[18]
	ν(C-O)		1385		1364[16]
	$\rho_{\perp}(CH_3)$	1051		1051	1052[20], 1049[18]
	$\rho_{\parallel}(CH_3)$	1029		1023	1025[20], 1026[18]

[a] Peak observed with negative intensity

on the surface. However, a peak at 1741 cm^{-1} does remain in the SiO_2 surface spectrum, which is best explained by strong adsorption of a portion of acetic acid monomers to the surface.

The bands that remain in the spectrum for γ-Al_2O_3 after gas phase acetic acid has been evacuated contain information about the coordination of acetic acid adsorbed on the surface. Previous studies[19,16] of acetic acid on oxide surfaces have shown the bands at 1586 and 1479 cm^{-1} to be indicative of bidentate coordination to the surface as depicted in Figure 3.7a. The two bands at 1641 and 1329 cm^{-1} have also been shown to represent acetate with a monodentate coordination as shown in Figure 3.7b.[19,16]

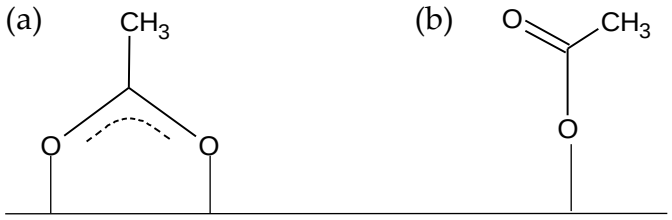

Figure 3.7. Visual depiction of acetic acid coordination on oxide surfaces. (a) Bidentate coordination and (b) monodentate coordination.

The surface spectra for CaO differed from that of γ-Al_2O_3 and SiO_2, displaying a band representing the acetic acid monomer at 1711 cm^{-1} in addition to a loss between 1400 and 1600 cm^{-1} due to carbonate species. Two important peaks at 1613 and 1335 cm^{-1} remain in the spectrum after evacuation of the gas

phase which represent the anti-symmetric and symmetric stretching modes of the COO^- group in carboxylic acid salts, suggesting the reaction of acetic acid with CaO to form calcium acetate and water as shown in equation 3.2.

$$CaO + 2CH_3COOH \rightarrow Ca(CH_3COO)_2 + H_2O \quad (3.2)$$

3.3.2. Determination of Saturation Coverage

The first step in determining the saturation coverage of acetic acid on the three mineral dust components studied involved calibrating the absorbance of the FT-IR spectra to coverage in units of molecules/cm^2. This is done by performing a blank experiment with a clean, dry tungsten grid in the sample chamber with no oxide sample present. In this experiment, the same pressures used in the saturation experiments were used, with the same experimental procedure as described for the saturation experiments. The pressure in the premix chamber before introducing the vapor to the sample cell was recorded, as well as the pressure after the 20 minute exposure to acetic acid. These values were also recorded during experimentation with the sample present. The pressure values for both the blank and experimental trials are then used in the calibration calculations.

For the calibration, the amount of acetic acid adsorption on the sample alone needs to be determined. This is done by subtracting the amount of adsorption on the walls of the sample cell and premix chamber, represented by

the change in pressure of the blank experiment, from the amount of adsorption on both the walls of the system and the sample, which is represented by the change in pressure of the actual experiment. These calculations are expressed in terms of pressure, shown by equations 3.3, 3.4, and 3.5.

$$P_{bl,i} - P_{bl,eq} = \Delta P_{bl} \tag{3.3}$$

$$P_{exp,i} - P_{exp,eq} = \Delta P_{exp} \tag{3.4}$$

$$\Delta P = \Delta P_{exp} - \Delta P_{bl} \tag{3.5}$$

where $P_{bl,i}$ is the initial blank pressure, $P_{bl,eq}$ is the equilibrium blank pressure, $P_{exp,i}$ is the initial experimental pressure, $P_{exp,eq}$ is the equilibrium experimental pressure and ΔP denotes the change in pressure that represents the amount of adsorption on only the sample surface. This change in pressure attributed to surface adsorption can then be used in conjunction with the ideal gas equation to determine the number of molecules adsorbed on the surface. It is important to note that this calibration is only done using the pressure difference for the first and lowest pressure of the experiment. After calculating the number of molecules adsorbed on the surface, a conversion factor with units of molecules AU^{-1} is calculated by dividing the number of molecules adsorbed on the surface by the integrated absorbance or peak height of the vibrational modes of interest using the spectrum collected at the lowest pressure. This conversion factor is then used to determine the number of molecules adsorbed on the surface based

on the integrated absorbance or peak height of the vibrational modes of interest. In order to get comparable values between each experimental trial, surface coverage must be calculated by dividing the number of molecules adsorbed by the total surface area of the sample for that trial, which is calculated by multiplying the mass of the sample by the BET surface area.

The calculated surface coverage versus pressure for acetic acid on each component has been plotted in figures 3.8, 3.9, and 3.10. It is clear that for all three components, surface coverage increases rapidly as pressure increases in the lower pressure region before leveling off, resembling a Type I isotherm, which accounts for monolayer adsorption. Using this information, the three-parameter BET equation (3.6) was reduced to the Langmuir equation (3.7) when n = 1.

$$V = \frac{V_m c\left(\frac{P}{P_0}\right)}{1-\left(\frac{P}{P_0}\right)} \frac{1-(n+1)\left(\frac{P}{P_0}\right)^n+n\left(\frac{P}{P_0}\right)^{n+1}}{1+(c-1)\left(\frac{P}{P_0}\right)-c\left(\frac{P}{P_0}\right)^{n+1}} \tag{3.6}$$

$$V = \frac{V_m c\left(\frac{P}{P_0}\right)}{1+c\left(\frac{P}{P_0}\right)} \tag{3.7}$$

$$\frac{P}{N} = \frac{1}{N_s K} + \frac{P}{N_s} \tag{3.8}$$

The Langmuir equation could then be further simplified and put in a linear form as shown by equation (3.8), where P is pressure, N is surface coverage, N_s is saturation coverage, K is the Langmuir constant, and c is a temperature

dependent constant related to the standard enthalpies of adsorption of the first and higher layers which can be calculated using the equation $c = e^{-[\Delta H_1 - \Delta H_2/RT]}$.

Plotting pressure divided by coverage versus pressure shows a linear relationship as shown in figures 3.8b, 3.9b, and 3.10b. The best-fit linear equation for these data points can then be correlated to the simplified linear version of the Langmuir equation discussed previously (Eq. 3.9), where the slope can be defined as the inverse of saturation coverage (N_s) and the intercept as the inverse of the quantity saturation coverage times Langmuir constant as shown in the following equations (3.10 and 3.11).

$$\text{Slope} = \frac{1}{N_S} \longrightarrow N_s = \frac{1}{\text{slope}} \tag{3.10}$$

$$\text{Intercept} = \frac{1}{N_S K} \tag{3.11}$$

3.4. Conclusions

After completing the calibration described in the previous section for each component the saturation coverages of each sample were calculated, resulting in the values displayed in Table 3.4. The result of high saturation coverage on CaO and low saturation coverage on SiO_2 is consistent with a previous study investigating the adsorption of nitric acid on these components.[11] The high adsorption of acetic acid on CaO, despite having the lowest surface area, can be explained by interaction of acid with a few layers of the bulk material as well as

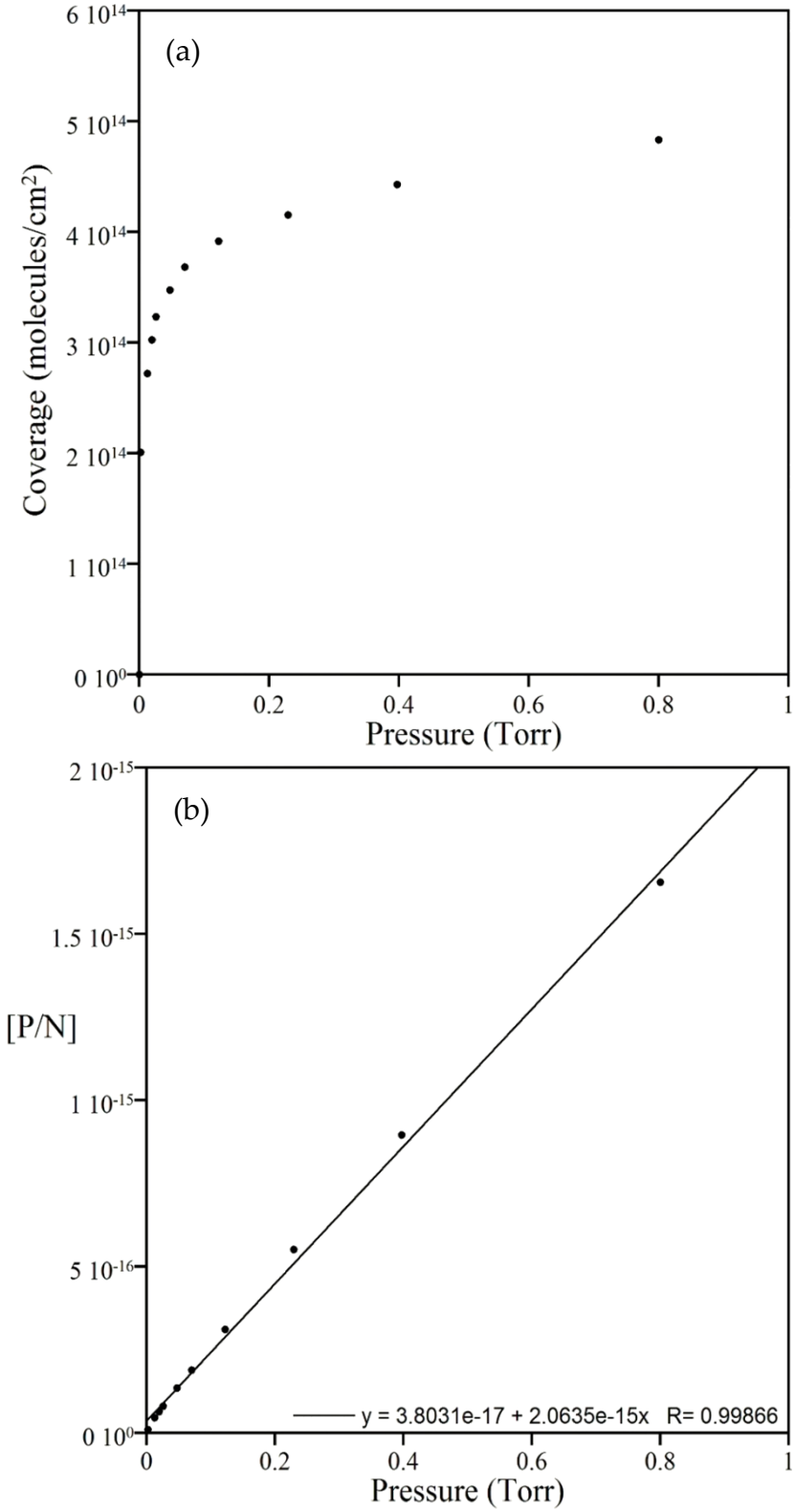

Figure 3.8. Plots used to calculate saturation coverage. (a) Calculated surface coverage versus pressure and (b) [P/N] versus pressure for γ-Al_2O_3 using peak height of band at 1586 cm^{-1}.

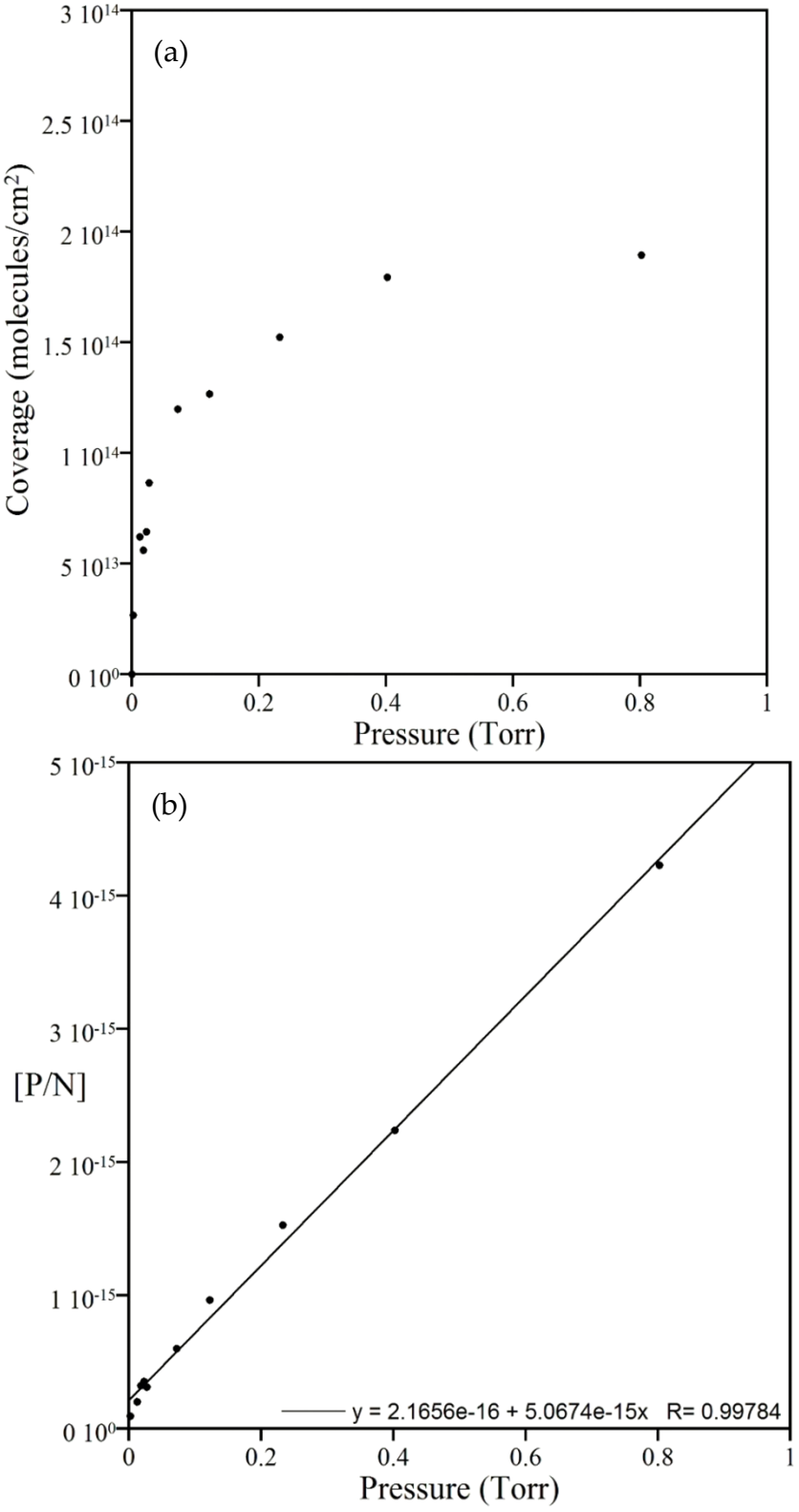

Figure 3.9. Plots used to calculate saturation coverage. (a) Calculated surface coverage versus pressure and (b) [P/N] versus pressure for SiO_2 using the integrated area of the C=O stretching modes.

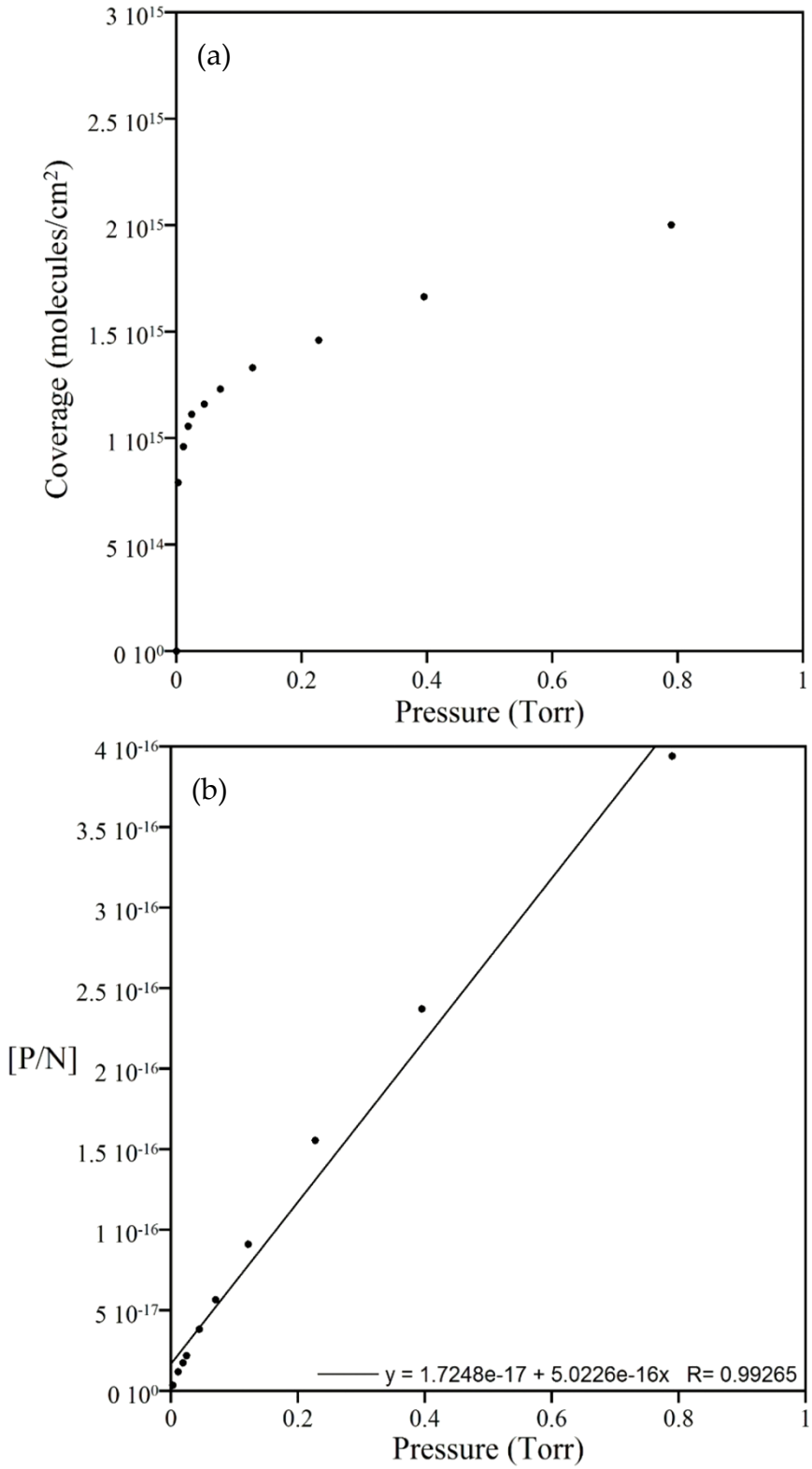

Figure 3.10. Plots used to calculate saturation coverage. (a) Calculated surface coverage versus pressure and (b) [P/N] versus pressure for CaO using the integrated area of peaks at 1613 and 1711 cm^{-1}.

the strong reaction occurring on the surface layer to create the carboxylic acid salt, calcium acetate.[11]

Table 3.4. Saturation coverage of acetic acid on γ-Al_2O_3, SiO_2 and CaO.

Sample	Saturation Coverage (molecules/cm^2)
γ-Al_2O_3	$(4.8 \pm 0.1) \times 10^{14}$
SiO_2	$(1.97 \pm 0.04) \times 10^{14}$
CaO	$(1.99 \pm 0.08) \times 10^{15}$

From the saturation studies described previously, it was determined that acetic acid adsorption on γ-Al_2O_3 and CaO is an irreversible process, while adsorption of acetic acid on SiO_2 is a reversible process. After analysis of the FT-IR surface spectra, it was determined that acetic acid adsorbed on the γ-Al_2O_3 surface has both monodentate and bidentate coordination to the surface. In contrast, acetic acid maintains monodentate coordination on the CaO surface.

CHAPTER 4

REACTION KINETICS OF ACETIC ACID ON γ-Al_2O_3 UNDER DRY CONDITIONS AND EFFECT OF RELATIVE HUMIDITY ON UPTAKE

4.1. Introduction

The effect of relative humidity on the uptake of trace atmospheric gases, including acids, is an important aspect to consider due to the abundance of water vapor present in the atmosphere. Previous studies regarding the effect of relative humidity on nitric acid uptake on various proxies of components of mineral dust aerosol have shown that nitric acid uptake is enhanced by up to 50 times when water vapor is present.[11] This study aimed to investigate whether this trend of enhanced acid uptake in the presence of water vapor holds true for other acids, such as organic acids, in the atmosphere.

4.2. Experimental Procedure

4.2.1. Kinetics Experiments under Dry Conditions

For kinetics studies, the procedure for preparing the sample, evacuating the system and preparing the acetic acid vapor in the premix chamber remained the same as for the saturation studies. However, once the pressure within the premix chamber was stable, a macro was used to collect spectra at a faster rate, every 2.5 seconds, for a duration of 20 minutes. In order to minimize time between spectra, only four scans were collected per spectrum. Due to the speed

of the reaction as well as collection of spectra, no background spectra of the tungsten mesh grid were collected. Taking the ratio of the single beam spectra during experimentation and the single beam spectrum collected before experimentation provides a transmittance spectrum which can then be converted to an absorbance spectrum of the sample surface with the gas phase present using the relationship between percent transmittance and absorbance described in Chapter 2. After 20 minutes, spectra of both the sample and tungsten grid were collected to get an absorbance spectrum of the sample surface with the gas phase subtracted as was done with the spectra collected before experimentation under vacuum. The peak height of the $\nu(COO)_{as}$ mode of each spectrum was recorded. These values were then converted to units of molecules cm^{-2} using the calibration procedure and calculations described in Chapter 3. Once in units of molecules cm^{-2}, quantitative values such as uptake coefficient and rate of adsorption can be determined.

4.2.2. Kinetics Experiments in the Presence of Water

To study the effect of relative humidity on the uptake of acetic acid, a procedure similar to that of the dry kinetics studies was utilized, along with the same sample preparation procedure as described previously. A predetermined acetic acid vapor pressure was first introduced to the isolated premix chamber and allowed to stabilize before adding water vapor at various pressures

corresponding to 5-15% relative humidity (~1-3 Torr). This mixture was then immediately introduced to the sample cell to reduce the amount of reaction between the two vapors before entering the cell. The pressure within the system was recorded at the time the mixture was introduced and a macro was used to collect spectra (one scan per spectrum) continuously for approximately 20 minutes with a resolution of 8 cm^{-1}. Absorbance spectra of the surface during the reaction were calculated and the peak height of the $\nu(COO)_{as}$ mode was used as described in the previous experimental procedure to calculate and compare uptake coefficients of acetic acid on mineral aerosols under dry conditions to those with water vapor present. FT-IR spectra of the γ-Al_2O_3 surface at the three different acetic acid pressures in the presence of 5% relative humidity are displayed in the Appendix. These spectra show that the same features are present as when under dry conditions.

4.3. Results and Discussion

In comparing kinetics data for both dry and wet experiments, uptake coefficients were calculated. Uptake coefficient is defined by equation 4.1 where the numerator is the rate of adsorption and the denominator is the impingement rate, or flux. Flux can be calculated using equation 4.2, where *P* is the pressure of acetic acid, *N* is Avogadro's number, *M* is the molecular weight of the gas, *R* is the gas constant and *T* is temperature. Rate of adsorption can be defined

mathematically by equation 4.3 where k is the rate constant of adsorption, $(1-\theta)$ is the number of available sites for reaction on the particle surface and $\theta = N_a/N_s$ (N_s is saturation coverage of acetic acid on the oxide particles), and P is the pressure of acetic acid vapor.

$$\gamma = \frac{\left(\frac{dN_a}{dt}\right)}{\text{Flux}} \tag{4.1}$$

$$\text{Flux} = \frac{PN}{(2\pi MRT)^{1/2}} \tag{4.2}$$

$$\frac{dN_a}{dt} = k(1-\theta)N_sP \tag{4.3}$$

However, making the assumptions that pressure, P, is constant and that the number of surface sites available for reaction is large compared to the number of species bound to the surface (i.e. $(1-\theta) >> \theta$), the slope of the initial linear portion of the coverage versus time plots is proportional to the rate of adsorption. Therefore, this slope can be used as the rate of adsorption when calculating the uptake coefficient.

FT-IR absorbance spectra of experiments performed under dry conditions at each acetic acid pressure, 70, 150 and 300 mTorr, are shown in Figures 4.1, 4.2 and 4.3. Comparing these spectra to the surface spectra collected during the saturation experiments there are some clear similarities and differences. All of the same peaks remain in the spectrum, however, there is some peak shifting in

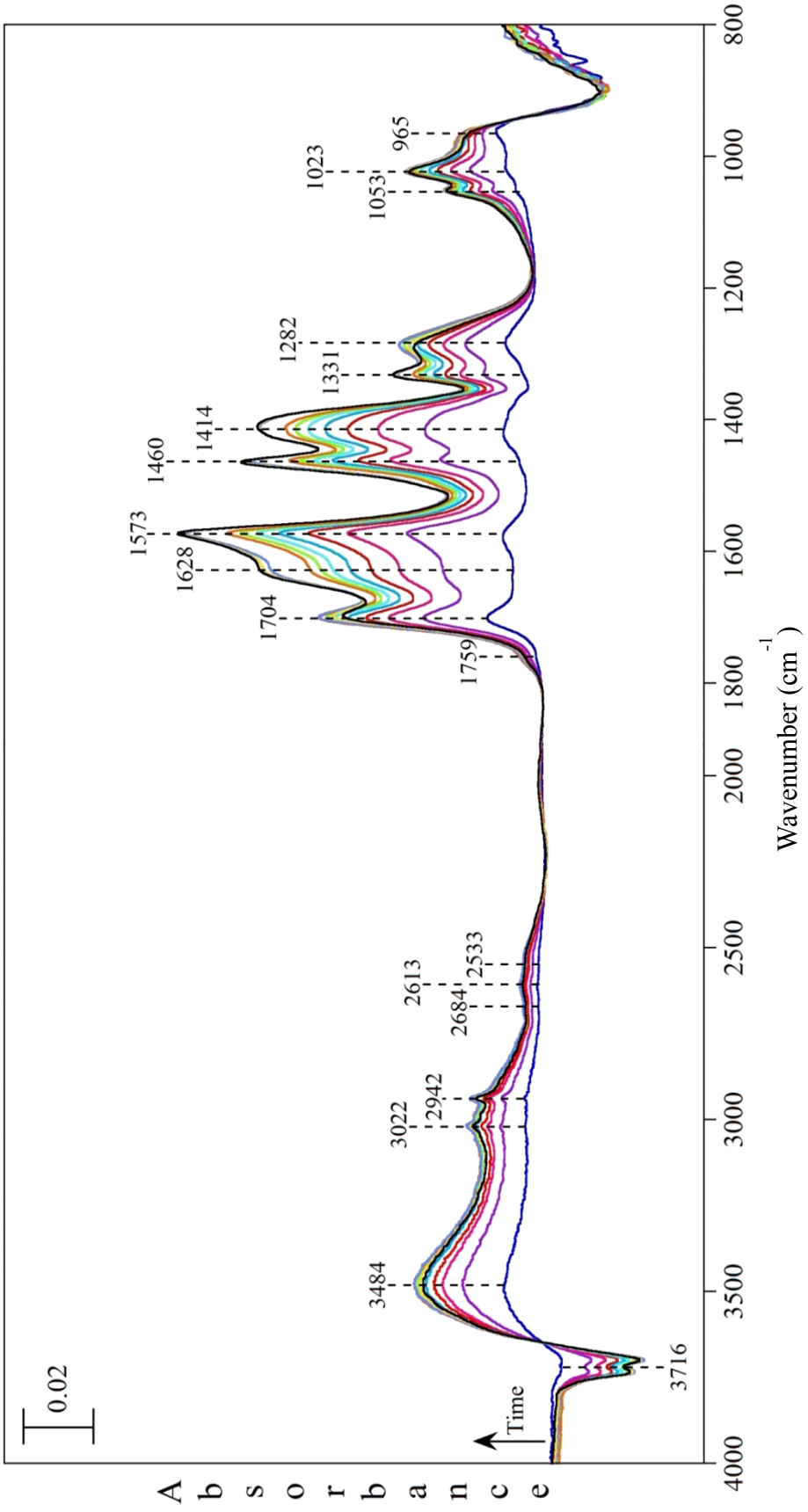

Figure 4.1. Absorbance FT-IR spectra of acetic acid adsorption, 70 mTorr, on γ-Al_2O_3 with increasing time.

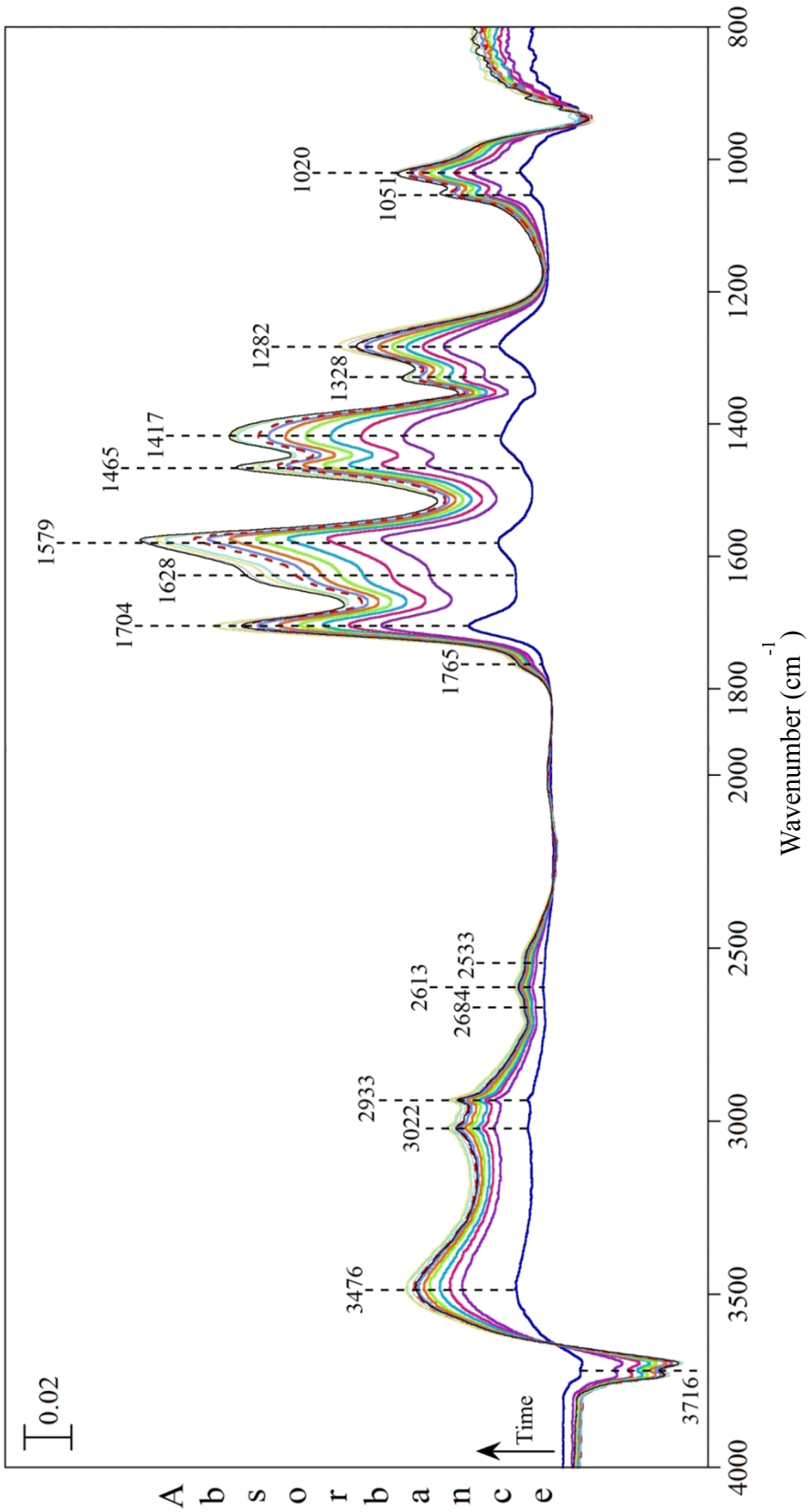

Figure 4.2. Absorbance FT-IR spectra of acetic acid adsorption, 150 mTorr, on γ-Al_2O_3 with increasing time.

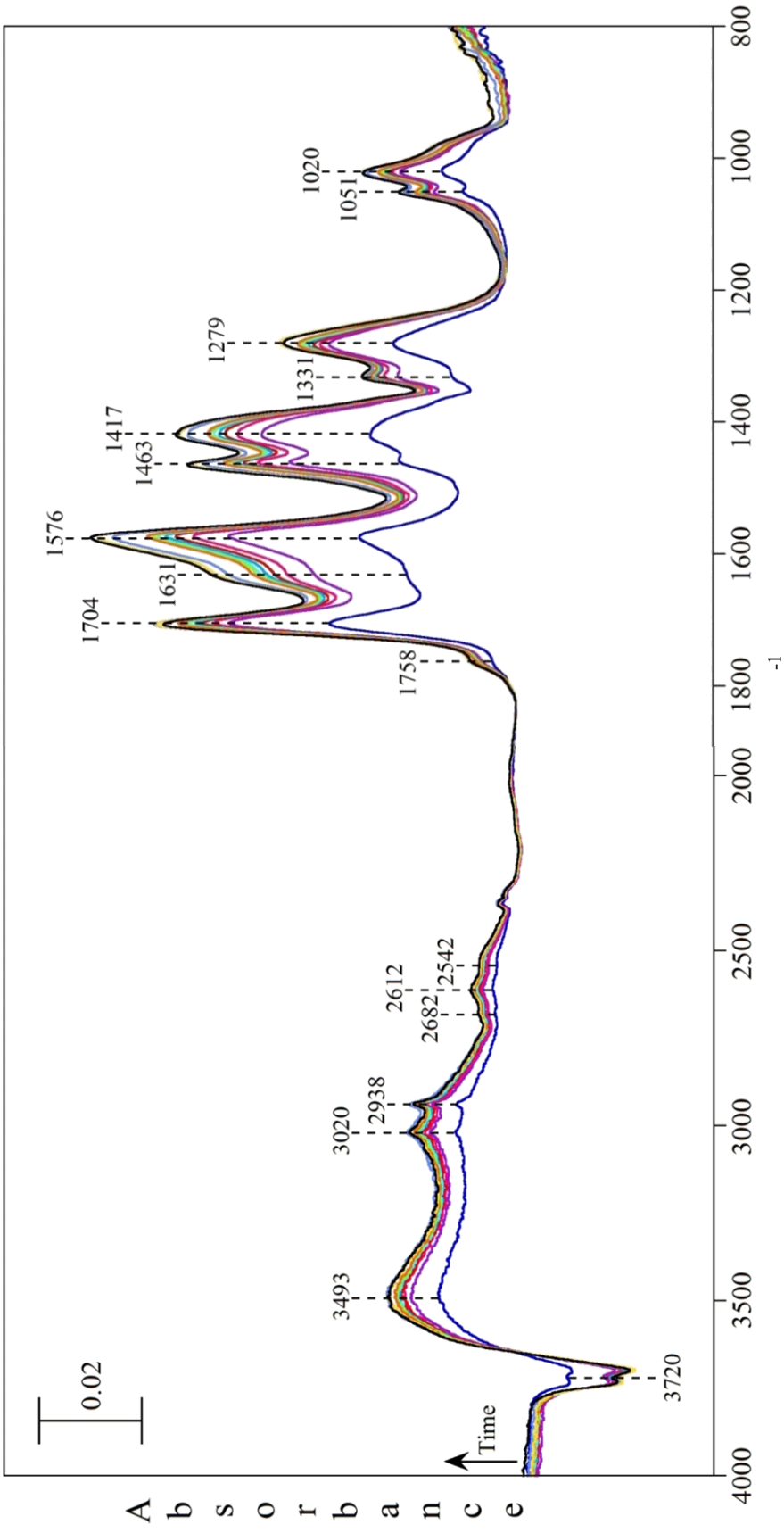

Figure 4.3. Absorbance FT-IR spectra of acetic acid adsorption, 300 mTorr, on γ-Al_2O_3 with increasing time.

Table 4.1. Kinetics analysis of acetic acid uptake averages on γ-Al_2O_3 under dry conditions and in the presence of water vapor.

Pressure (mTorr)	% RH	Rate (molecules cm^{-2})	Flux (molecules cm^{-2})	Uptake Coefficient (γ)	$\frac{\gamma_{wet}}{\gamma_{dry}}$
70	0	3.1×10^{12}	1.8×10^{19}	$(2 \pm 0.2) \times 10^{-7}$	
70	5	1.7×10^{13}	1.8×10^{19}	$(9 \pm 3) \times 10^{-7}$	5
70	10	1.9×10^{13}	1.8×10^{19}	$(1 \pm 0.3) \times 10^{-6}$	6
70	15	1.7×10^{13}	1.8×10^{19}	$(9 \pm 4) \times 10^{-7}$	6
150	0	9.7×10^{12}	3.9×10^{19}	$(2 \pm 0.5) \times 10^{-7}$	
150	5	3.7×10^{13}	3.9×10^{19}	$(9 \pm 3) \times 10^{-7}$	4
150	10	3.0×10^{13}	3.9×10^{19}	$(8 \pm 3) \times 10^{-7}$	3
150	15	4.1×10^{13}	3.9×10^{19}	$(1 \pm 0.5) \times 10^{-6}$	4
300	0	2.0×10^{13}	7.9×10^{19}	$(3 \pm 2) \times 10^{-7}$	
300	5	5.8×10^{13}	7.9×10^{19}	$(7 \pm 3) \times 10^{-7}$	3
300	10	6.8×10^{13}	7.9×10^{19}	$(9 \pm 6) \times 10^{-7}$	3
300	15	7.1×10^{13}	7.9×10^{19}	$(9 \pm 5) \times 10^{-7}$	4

comparison to the surface spectra. The C=O stretching peaks of the acetic acid monomer and dimer are clearly represented by the bands around 1760 and 1704 cm^{-1} respectively. Looking at the acetic acid dimer peak at 1704 cm^{-1} and comparing the three different acetic acid pressures it is clear that the maximum peak height increases as the acetic acid pressure increases, indicating an increased presence and adsorption of the acetic acid dimer.

The average rates and uptake coefficients were determined as shown in Table 4.1, with results from each experiment being displayed in the Appendix. Comparing uptake coefficients for acetic acid uptake under dry conditions, uptake increases slightly as acetic acid pressure increases. However, it could also be interpreted that uptake coefficient for acetic acid on γ-Al_2O_3 under dry conditions is independent of pressure due to the similarity in uptake coefficient values at each pressure. Since water vapor is always present in the atmosphere, it is important to consider the effect that water vapor has on the uptake of acetic acid on the surface of mineral dust particles. In comparison to uptake coefficients calculated for dry conditions, it was determined that the presence of water enhances the uptake of acetic acid on the surface. The acetic acid uptake is anywhere from three to six times higher when water vapor is present. However, the combinations of acetic acid pressure and relative humidity studied showed no direct correlation between relative humidity and uptake.

4.4. Conclusions

Upon completion of studies investigating the uptake of acetic acid on γ-Al_2O_3 under both dry and humid conditions it was discovered that uptake of acetic acid is enhanced under conditions of increased relative humidity. Compared to the enhancement observed of nitric acid uptake in the presence of relative humidity, the enhancement of acetic acid uptake is much less, increasing by only three to six times as compared to up to 50-fold for nitric acid.[11] It was also observed that the enhancement of acetic acid uptake on the surface decreased in magnitude as the pressure of acetic acid increased from 70 to 300 mTorr.

CHAPTER 5

CONCLUSION

The reaction of acetic acid on three different components of mineral dust aerosol, γ-Al_2O_3, SiO_2 and CaO, was studied. Through these studies, it was determined that acetic acid irreversibly adsorbs on γ-Al_2O_3 and CaO surfaces, while reversibly adsorbing on SiO_2. Strongly adsorbed acetic acid on γ-Al_2O_3 has both monodentate and bidentate coordination. The strong adsorption of acetic acid on CaO was found to have a monodentate coordination on the surface. In terms of saturation coverage, SiO_2 was found to have the lowest saturation coverage, with CaO having the highest saturation coverage. This result agreed with a previous work which explained the high saturation coverage on CaO as being due to a strong surface reaction and interaction with bulk layers.[11]

The uptake kinetics of acetic acid on γ-Al_2O_3 was also investigated at three different pressures, 70, 150 and 300 mTorr. From these studies it was determined that there is little to no dependence of acetic acid pressure on uptake, with uptake coefficients ranging from 2×10^{-7} to 3×10^{-7}. The effect of water vapor on acetic acid uptake is an important relationship to study due to the abundance of water vapor in the atmosphere. When investigating this relationship, three different relative humidities were studied at each of the three acetic acid pressures studied under dry conditions in order to obtain an accurate

comparison of wet versus dry conditions. Upon completion of these studies it was determined that the presence of water vapor enhances acetic acid uptake by a factor of three to six. Comparing the ratio of wet and dry uptake coefficients displays a trend where the presence of water vapor has a lower effect on acetic acid uptake as acetic acid pressure increases.

Although the reactions occurring at the surfaces of particles in the atmosphere are complex, these results have provided insight into some of the reactions that occur. With the amount of organic acids being emitted into the atmosphere from sources such as motor exhaust, the interaction between mineral dust aerosol and acetic acid is of particular importance. The results of this study have provided information regarding the strength of adsorption of acetic acid on various surfaces and rate at which acetic acid is adsorbed on the γ-Al_2O_3 surface, which in turn offers information about the structure of reacted mineral dust particles in the atmosphere. In conjunction with additional studies, the results displayed within this work could provide a deeper understanding of how mineral dust particles and trace atmospheric gases interact in the atmosphere.

APPENDIX

Table A.1. Kinetics analysis of acetic acid uptake on γ-Al_2O_3 under dry conditions and in the presence of water vapor.

Pressure (mTorr)	% RH	Rate (molecules cm^{-2})	Flux (molecules cm^{-2})	Uptake Coefficient (γ)
70	0	5.3×10^{12}	1.8×10^{19}	$(3 \pm 0.4) \times 10^{-7}$
70	0	8.5×10^{11}	1.8×10^{19}	$(5 \pm 0.8) \times 10^{-8}$
70	4.7	1.3×10^{13}	1.8×10^{19}	$(7 \pm 1) \times 10^{-7}$
70	7.1	2.1×10^{13}	1.8×10^{19}	$(1 \pm 0.4) \times 10^{-6}$
70	10.2	2.2×10^{13}	1.8×10^{19}	$(1 \pm 0.4) \times 10^{-6}$
70	9.9	1.7×10^{13}	1.8×10^{19}	$(9 \pm 2) \times 10^{-7}$
70	14.8	1.9×10^{13}	1.8×10^{19}	$(1 \pm 0.4) \times 10^{-6}$
70	14.8	1.5×10^{13}	1.8×10^{19}	$(8 \pm 3) \times 10^{-7}$
150	0	8.6×10^{12}	3.9×10^{19}	$(2 \pm 0.4) \times 10^{-7}$
150	0	1.1×10^{13}	3.9×10^{19}	$(3 \pm 0.5) \times 10^{-7}$
150	5.1	4.2×10^{13}	3.9×10^{19}	$(1 \pm 0.4) \times 10^{-6}$
150	4.8	3.2×10^{13}	3.9×10^{19}	$(8 \pm 2) \times 10^{-7}$
150	9.5	2.6×10^{13}	3.9×10^{19}	$(7 \pm 3) \times 10^{-7}$
150	11.2	3.5×10^{13}	3.9×10^{19}	$(9 \pm 4) \times 10^{-7}$
150	15.4	5.1×10^{13}	3.9×10^{19}	$(1 \pm 0.6) \times 10^{-6}$
150	14.9	3.1×10^{13}	3.9×10^{19}	$(8 \pm 3) \times 10^{-7}$
300	0	1.6×10^{13}	7.9×10^{19}	$(2 \pm 2) \times 10^{-7}$
300	0	2.3×10^{13}	7.9×10^{19}	$(3 \pm 1) \times 10^{-7}$
300	5.2	8.2×10^{13}	7.9×10^{19}	$(1 \pm 0.3) \times 10^{-6}$
300	4.8	3.5×10^{13}	7.9×10^{19}	$(4 \pm 3) \times 10^{-7}$
300	10.2	8.5×10^{13}	7.9×10^{19}	$(1 \pm 0.7) \times 10^{-6}$
300	10.1	5.1×10^{13}	7.9×10^{19}	$(6 \pm 5) \times 10^{-7}$
300	15	8.6×10^{13}	7.9×10^{19}	$(1 \pm 0.5) \times 10^{-6}$
300	14.9	5.6×10^{13}	7.9×10^{19}	$(7 \pm 4) \times 10^{-7}$

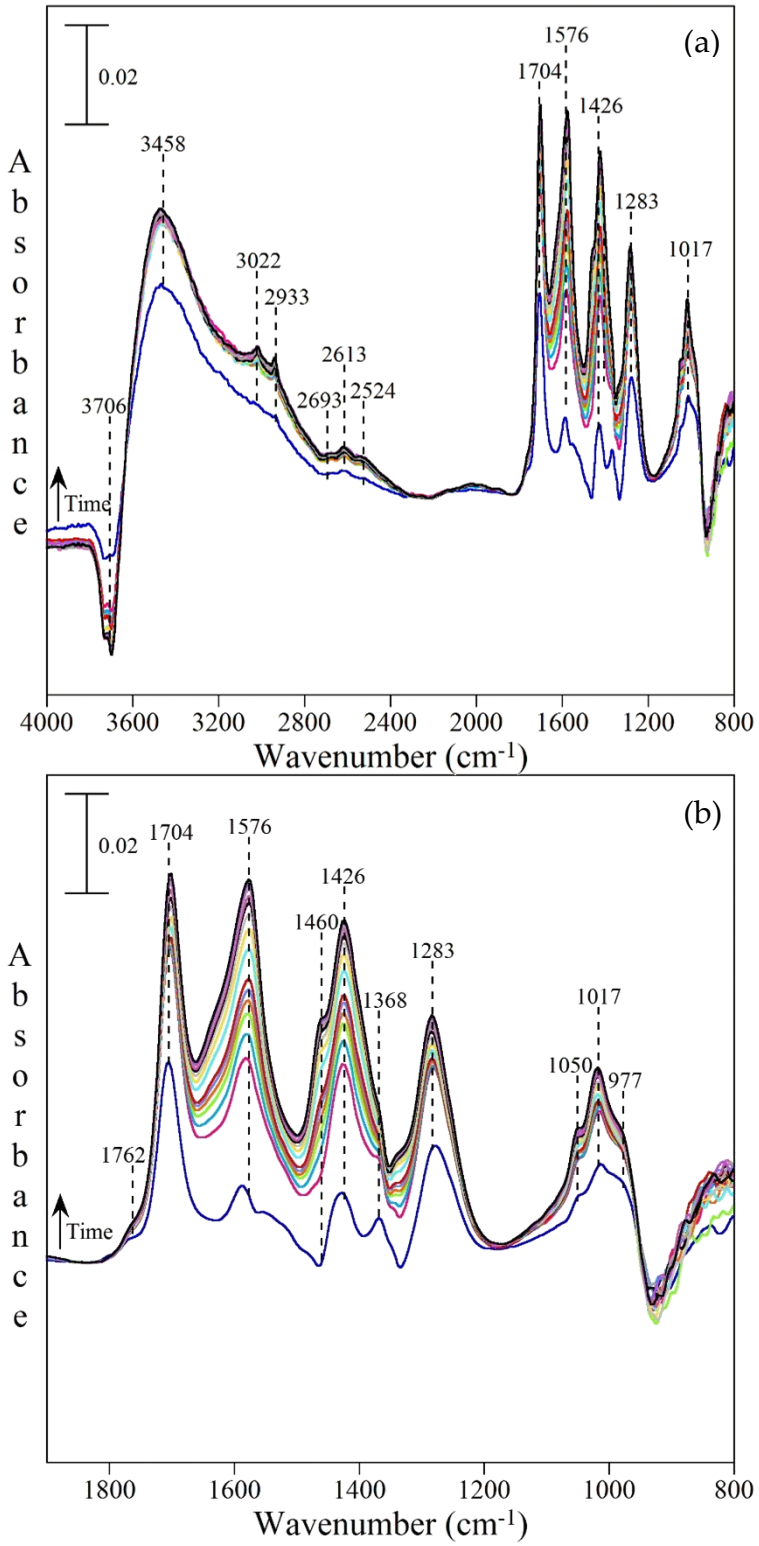

Figure A.1. FT-IR spectra of γ-Al_2O_3 in presence of 70 mTorr acetic acid and 5% relative humidity. (a) Full spectral range (800-4000 cm^{-1}) and (b) 800-1900 cm^{-1}.

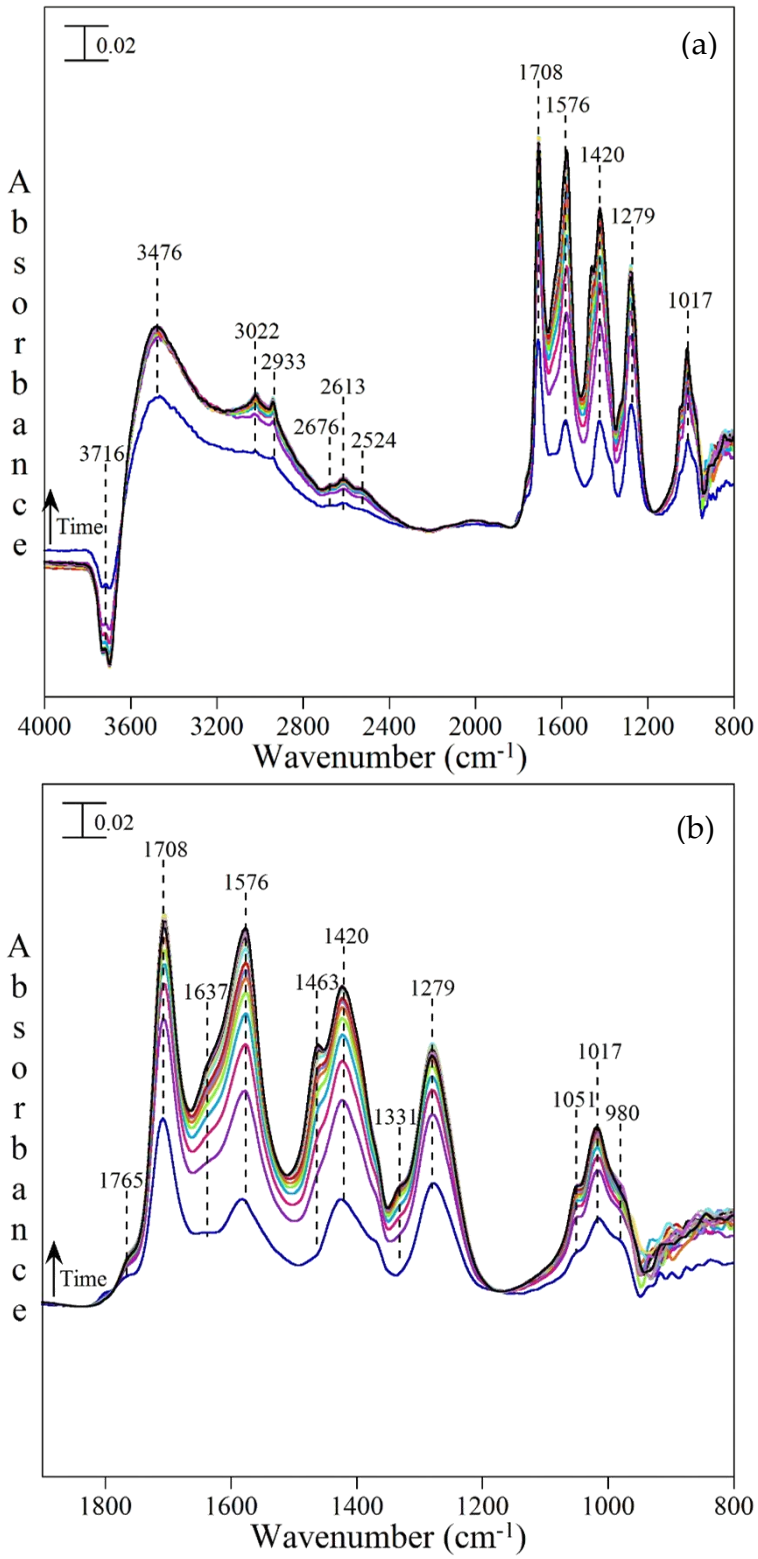

Figure A.2. FT-IR spectra of γ-Al_2O_3 in presence of 150 mTorr acetic acid and 5% relative humidity. (a) Full spectral range (800-4000 cm^{-1}) and (b) 800-1900 cm^{-1}.

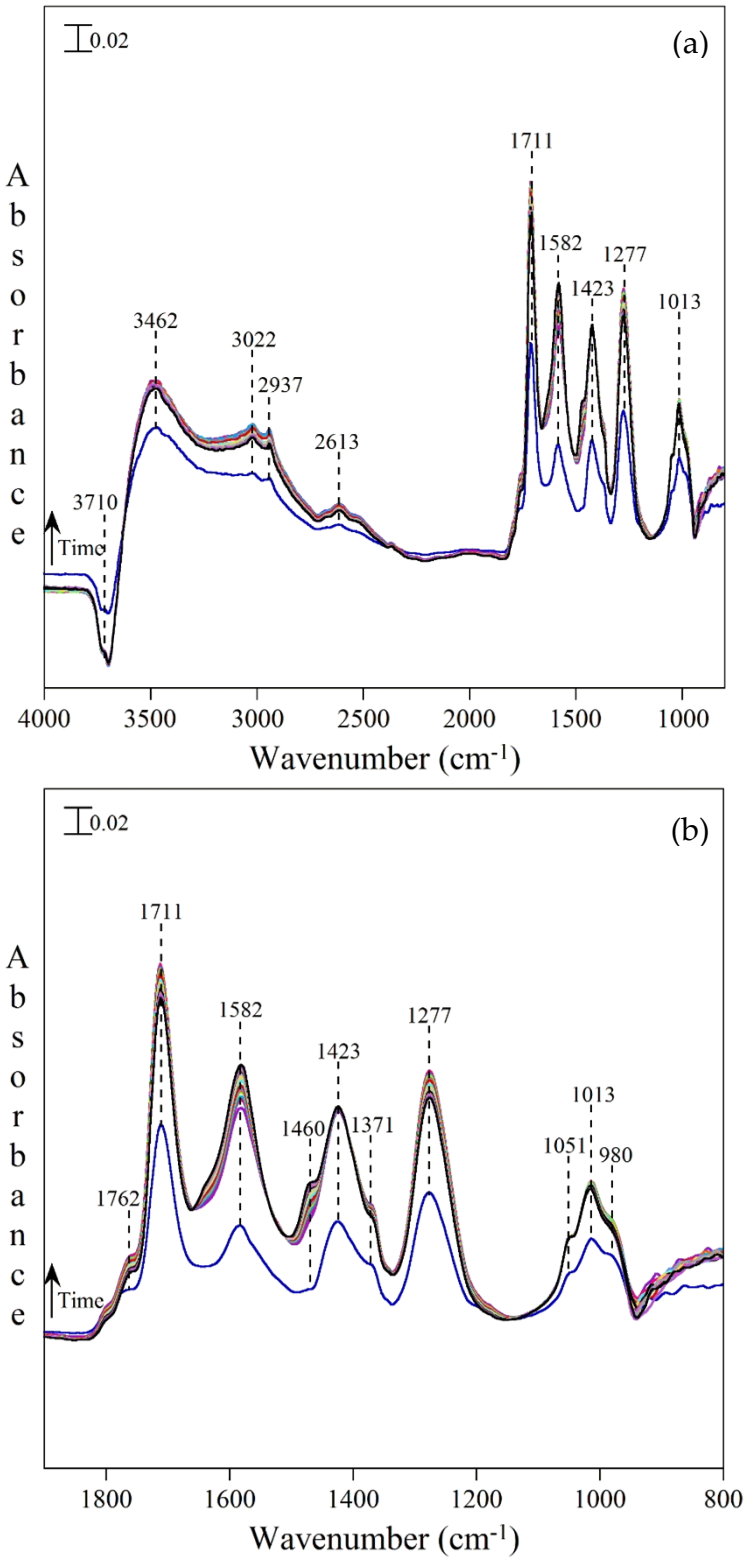

Figure A.3. FT-IR spectra of γ-Al_2O_3 in presence of 300 mTorr acetic acid and 5% relative humidity. (a) Full spectral range (800-4000 cm^{-1}) and (b) 800-1900 cm^{-1}.

REFERENCES

1. Tong, S. R.; Wu, L. Y.; Ge, M. F.; Wang, W. G.; Pu, Z. F., Heterogeneous chemistry of monocarboxylic acids on alpha-Al_2O_3 at different relative humidities. *Atmospheric Chemistry and Physics* **2010,** *10* (16), 7561-7574.

2. Tegen, I.; Fung, I., Modeling of mineral dust in the atmosphere - Sources, transport, and optical thickness. *Journal of Geophysical Research-Atmospheres* **1994,** *99* (D11), 22897-22914.

3. Dalmeida, G. A., On the variability of desert aerosol radiative characteristics. *Journal of Geophysical Research-Atmospheres* **1987,** *92* (D3), 3017-3026.

4. Dentener, F. J.; Carmichael, G. R.; Zhang, Y.; Lelieveld, J.; Crutzen, P. J., Role of mineral aerosol as a reactive surface in the global troposphere. *Journal of Geophysical Research-Atmospheres* **1996,** *101* (D17), 22869-22889.

5. Li, X.; Maring, H.; Savoie, D.; Voss, K.; Prospero, J. M., Dominance of mineral dust in aerosol light-scattering in the North Atlantic trade winds. *Nature* **1996,** *380* (6573), 416-419.

6. Prospero, J. M., Long-range transport of mineral dust in the global atmosphere: Impact of African dust on the environment of the southeastern United States. *Proceedings of the National Academy of Sciences of the United States of America* **1999,** *96* (7), 3396-3403.

7. Sheehy, D. P., A perspective on desertification of grazing-land ecosystems in North China. *Ambio* **1992,** *21* (4), 303-307.

8. Charlson, R. J.; Schwartz, S. E.; Hales, J. M.; Cess, R. D.; Coakley, J. A.; Hansen, J. E.; Hofmann, D. J., Climate forcing by anthropogenic aerosols. *Science* **1992,** *255* (5043), 423-430.

9. Prather, K. A.; Hatch, C. D.; Grassian, V. H., Analysis of atmospheric aerosols. *Annual Review of Analytical Chemistry* **2008,** *1*, 485-514.

10. Zhang, Y.; Young, S. W.; Kotamarthi, V.; Carmichael, G. R., Photochemical oxidant processes in the presence of dust - An evaluation of the impact of dust on particulate nitrate and ozone formation. *Journal of Applied Meteorology* **1994,** *33* (7), 813-824.

11. Goodman, A. L.; Bernard, E. T.; Grassian, V. H., Spectroscopic study of nitric acid and water adsorption on oxide particles: Enhanced nitric acid uptake kinetics in the presence of adsorbed water. *Journal of Physical Chemistry A* **2001,** *105* (26), 6443-6457.

12. Rubasinghege, G.; Ogden, S.; Baltrusaitis, J.; Grassian, V. H., Heterogeneous uptake and adsorption of gas-phase formic acid on oxide and clay particle surfaces: The roles of surface hydroxyl groups and adsorbed water in formic acid adsorption and the impact of formic acid adsorption on water uptake. *Journal of Physical Chemistry A* **2013,** *117* (44), 11316-11327.

13. Chebbi, A.; Carlier, P., Carboxylic acids in the troposphere, occurrence, sources, and sinks: A review. *Atmospheric Environment* **1996,** *30* (24), 4233-4249.

14. Talbot, R. W.; Beecher, K. M.; Harriss, R. C.; Cofer, W. R., Atmospheric geochemistry of formic and acetic acids at a mid-latitude temperate site. *Journal of Geophysical Research-Atmospheres* **1988,** *93* (D2), 1638-1652.

15. Galhotra, P., Carbon dioxide adsorption on nanomaterials. Ph.D. Dissertation, University of Iowa, Iowa City, IA, **2010**.

16. Xu, C.; Koel, B. E., Adsorption and reaction of CH_3COOH and CD_3COOD on the MgO(100) surface: A Fourier transform infrared and temperature programmed desorption study. *The Journal of Chemical Physics* **1995,** *102* (20), 8158.

17. Shimanouchi, T. *Tables of molecular vibrational frequencies consolidated Volume I*; National Bureau of Standards: 1972.

18. Hasan, M. A.; Zaki, M. I.; Pasupulety, L., Oxide-catalyzed conversion of acetic acid into acetone: an FTIR spectroscopic investigation. *Applied Catalysis a-General* **2003,** *243* (1), 81-92.

19. Pei, Z. F.; Ponec, V., On the intermediates of the acetic acid reactions on oxides: An IR study. *Applied Surface Science* **1996,** *103* (2), 171-182.

20. Finocchio, E.; Willey, R. J.; Busca, G.; Lorenzelli, V., FTIR studies on the selective oxidation and combustion of light hydrocarbons at metal oxide surfaces .3. Comparison of the oxidation of C-3 organic compounds over Co_3O_4, $MgCr_2O_4$ and CuO. *Journal of the Chemical Society-Faraday Transactions* **1997,** *93* (1), 175-180.